W and *Z* boson pair production at electron-positron colliders in gauge-Higgs unification

Naoki Yamatsu,[1,*] Shuichiro Funatsu,[2] Hisaki Hatanaka,[3] Yutaka Hosotani,[4] and Yuta Orikasa[5]

[1]*Department of Physics, National Taiwan University, Taipei, Taiwan 10617, Republic of China*
[2]*Ushiku, Ibaraki 300-1234, Japan*
[3]*Osaka, Osaka 536-0014, Japan*
[4]*Research Center for Nuclear Physics, Osaka University, Ibaraki, Osaka 567-0047, Japan*
[5]*Institute of Experimental and Applied Physics, Czech Technical University in Prague, Husova 240/5, 110 00 Prague 1, Czech Republic*

(Received 6 September 2023; accepted 10 November 2023; published 11 December 2023)

We examine W and Z boson pair production processes at electron-positron collider experiments in the $SU(3)_C \times SO(5)_W \times U(1)_X$ gauge-Higgs unification (GHU) model. We find that the deviation of the total cross section for the $e^-e^+ \to W^-W^+$ process from the Standard Model (SM) in the GHU model with parameter sets, which are consistent with the current experiments, is about 0.5% to 1.5% and 0.6% to 2.2% for $\sqrt{s} = 250$ GeV and 500 GeV, respectively, depending on the initial electron and positron polarization. We find that for the $e^-e^+ \to ZZ$ process the deviation from the SM in the GHU model is at most 1%. We find that unitarity bound for the $e^-e^+ \to W^-W^+$ process is satisfied in the GHU model as in the SM, as a consequence of the relationship among coupling constants.

DOI: 10.1103/PhysRevD.108.115014

I. INTRODUCTION

The Standard Model (SM) in particle physics has been established at low energies. However, it is not yet clear whether the observed Higgs boson has exactly the same properties as those in the SM. The Higgs couplings to quarks, leptons, and SM gauge bosons, as well as the Higgs self-coupling, need to be determined more accurately in future collider experiments such as the International Linear Collider (ILC) [1–6], the Compact Linear Collider (CLIC) [7], the Future Circular Collider (FCC-ee) [8], the Cool Copper Collider (C^3) [9], Circular Electron Positron Collider (CEPC) [10], and muon collider [11].

The SM Higgs boson sector has many problems, one of which is the fact that there are large corrections to the Higgs boson mass at the quantum level. Fine-tuning of the bare mass is required to obtain the observed Higgs mass $m_h = 125.25 \pm 0.17$ GeV [12]. One known way to stabilize the mass of the Higgs boson against quantum corrections is to identify the Higgs boson as a zero mode of the 5th dimensional component of the gauge potential. This scenario is called gauge-Higgs unification (GHU) [13–18]. In GHU models, the Higgs boson appears as a fluctuating mode in the Aharonov-Bohm (AB) phase θ_H in the 5th dimension; $SU(3)_C \times SO(5)_W \times U(1)_X$ GHU models in the Randall-Sundrum (RS) warped space have been proposed in Refs. [19–22], where $SO(5)_W \supset SU(2)_L \times SU(2)_R$. The GHU models are classified into two types, depending on whether quarks and leptons belong to the vector or the spinor representation of $SO(5)_W$. The GHU model whose quarks and leptons belong to the spinor representation of $SO(5)_W$ can be regarded as a low-energy effective description of the $SO(11)$ GHU model [23–29], where the SM gauge symmetry $SU(3)_C \times SU(2)_L \times U(1)_Y$ is embedded in the $SO(11)$ grand unified gauge symmetry [30–35] in higher dimensional framework [36–50]. The phenomena of the GHU model below the electroweak (EW) scale are very close to those of the SM in a parameter regime that satisfies the current experimental constraints on the Kaluza-Klein (KK) mass $m_{\rm KK} \gtrsim 13$ TeV and the AB phase $\theta_H \lesssim 0.1$ [22,51–58]. The strongest constraints come from the Large Hadron Collider (LHC) experiment at $\sqrt{s} = 13$ TeV with up to 140 fb^{-1} data [59–64] by using the Z' and W' boson search results for the $pp \to \ell\nu$ and $pp \to \ell^-\ell^+$ processes [55], where the Z' bosons are mixed vector bosons of $U(1)_X$, $U(1)_L (\subset SU(2)_L)$, and $U(1)_R (\subset SU(2)_R)$ and the W' bosons are mixed vector bosons of $SO(5)_W/(U(1)_L \times U(1)_R)$.

In the future e^-e^+ collider experiments, it is possible to explore up to the region of tens of TeV in terms of

*yamatsu@phys.ntu.edu.tw

the KK mass scale [53,56,57,65–78]. Large parity violation appears in the coupling of quarks and leptons to KK gauge bosons, especially to the first KK modes; the sign of the bulk mass parameter of the fermions in the GHU model is an important factor in determining whether the coupling constants of the Z' and W' bosons to the right- or left-handed fermions are larger. We studied observables such as cross sections and asymmetries [79–82] in the process of fermion pair production. Due to the very large cross section of the processes, we can clearly observe deviations from the SM in the early stage of the ILC experiment ($\sqrt{s} = 250$ GeV, integral luminosity $L_{\rm int} = 250$ fb^{-1}) even when $m_{\rm KK}$ is larger than the current experimental constraint $m_{\rm KK} \simeq 13$ TeV. The cross sections of the processes are very sensitive to the initial polarizations of the electron and the positron, so the sign of the corresponding bulk mass of each fermion in each final state in the GHU model can also be determined by analyzing the polarization dependence. Recently, we examined the single Higgs production processes such as the Higgs strahlung process $e^-e^+ \to Zh$ [57]. By using the Higgs strahlung process, it is possible to explore up to the region of tens of TeV in terms of the KK mass scale.

The vector boson pair production processes at e^-e^+ collider are significant. Measurements of the $W^\pm$ boson pair production process near the threshold are important for determining the W boson mass m_W. The deviation from the SM prediction has been recently reported by the Collider Detector at Fermilab (CDF) Collaboration at the Tevatron [83]. In the SM, the contributions to the $e^-e^+ \to W^-W^+$ process come from the s-channel process via γ and Z boson and the t-channel via neutrinos. In s-channel processes and t-channel processes alone, a factor s/m_W^2 appears in the cross section from the longitudinal polarization vector of the W boson in the final state. The unitarity bound on the high energy behavior of the total cross section is given by $\sigma_{\rm total} \le C\{\log(s)\}^2$, known as the Froissart bound [84,85], where C is a constant. For $s \gg m_W^2$, the total cross section may behave in such a way that unitarity is violated because each contribution from the s-channel and t-channel are $O(s)$. In the SM, individual cross sections that would break unitarity are miraculously canceled out by the cross sections between them because special conditions are satisfied between the coupling constants. As a result, the total cross section of $e^-e^+ \to W^-W^+$, which includes both s- and t-channel contributions, satisfies Froissart (unitarity) bound. This is required by the Goldstone boson equivalence theorem [86–88], where this theorem was first proofed in Ref. [86]. The proof of the theorem is based on the Ward identities of the spontaneously broken gauge theory. In Ref. [89], $W^\pm$ boson pair production has been partially analyzed in the LHC experiment, but not in the e^-e^+ collider, and the GHU model discussed in Ref. [89] is different from the GHU model discussed in the paper.

In this paper we analyze the W and Z boson pair production processes $e^-e^+ \to W^-W^+$ and $e^-e^+ \to ZZ$ in the GHU model to clarify the difference between the predictions in the SM and the GHU model. We show that unitarity bound for the $e^-e^+ \to W^-W^+$ process is satisfied in the GHU model as well as in the SM by investigating the asymptotic behavior of the cross sections for large $\sqrt{s}$. We calculate the energy and angle dependence of the cross sections and clarify the differences between the predictions of the SM and GHU models. We show that the $e^-e^+ \to W^-W^+$ process with $(\sqrt{s}, L_{\rm int}) = (250\ {\rm GeV}, 1\ {\rm ab}^{-1})$, $(500\ {\rm GeV}, 2\ {\rm ab}^{-1})$ at the ILC can explore up to the region of tens of TeV in terms of the KK mass scale, which is beyond the current constraints on the KK mass scale from the LHC experiment. We analyze the $e^-e^+ \to ZZ$ process in the same way and show that the deviation from the SM is at most 1%.

The paper is organized as follows. In Sec. II, the $SU(3)_C \times SO(5)_W \times U(1)_X$ GHU model is introduced. In Sec. III, we give some parameter sets of the GHU model. In Sec. IV, we give the formulas for the cross sections of the $e^-e^+ \to W^-W^+$ and $e^-e^+ \to ZZ$ processes, involving the Z' and W' bosons as well as the Z and W bosons. We show that unitarity bound in the $e^-e^+ \to W^-W^+$ process is satisfied in the GHU model. In Sec. V, we present numerical results for the cross sections of $e^-e^+ \to W^-W^+$ and $e^-e^+ \to ZZ$. Section VI is devoted to summary and discussions.

II. MODEL

In this paper, we focus on observables related with the EW gauge bosons and leptons at tree level. The $SU(3)_C$ gauge bosons and fermions except leptons are not directly involved, so we omit them. For the full field content in the GHU model, see Ref. [22], in which the $SU(3)_C \times SO(5)_W \times U(1)_X$ GHU model was originally proposed.

The GHU model is defined in the RS warped space with the following [90]:

$$ds^2 = g_{MN}dx^M dx^N = e^{-2\sigma(y)}\eta_{\mu\nu}dx^\mu dx^\nu + dy^2, \quad (2.1)$$

where $M,N = 0,1,2,3,5$, $\mu,\nu = 0,1,2,3$, $y = x^5$, $\eta_{\mu\nu} = {\rm diag}(-1,+1,+1,+1)$, $\sigma(y) = \sigma(y+2L) = \sigma(-y)$, and $\sigma(y) = ky$ for $0 \le y \le L$. By using the conformal coordinate $z = e^{ky}$ $(1 \le z \le z_L = e^{kL})$ in the region $0 \le y \le L$, the metric is rewritten by

$$ds^2 = \frac{1}{z^2}\left(\eta_{\mu\nu}dx^\mu dx^\nu + \frac{dz^2}{k^2}\right). \quad (2.2)$$

The bulk region $0 < y < L$ $(1 < z < z_L)$ is anti–de Sitter (AdS) spacetime with a cosmological constant $\Lambda = -6k^2$, which is sandwiched by the UV brane at $y = 0$ $(z = 1)$ and

the IR brane at $y = L$ $(z = z_L)$. The KK mass scale is $m_{\rm KK} = \pi k/(z_L - 1)$.

The $SO(5)_W \times U(1)_X$ symmetry includes the EW symmetry $SU(2)_L \times U(1)_Y$, where $SO(5)_W \supset SU(2)_L \times SU(2)_R$. $A_M^{SO(5)_W}$ and $A_M^{U(1)_X}$ represent the $SO(5)_W$ and $U(1)_X$ gauge fields, respectively. The orbifold boundary conditions (BCs) $P_j (j = 0, 1)$ of the gauge fields on the UV brane $(y = 0)$ and the IR brane $(y = L)$ are given by

$$\begin{pmatrix} A_\mu \\ A_y \end{pmatrix}(x, y_j - y) = P_j \begin{pmatrix} A_\mu \\ -A_y \end{pmatrix}(x, y_j + y) P_j^{-1} \tag{2.3}$$

for each gauge field, where $(y_0, y_1) = (0, L)$. For the $U(1)_X$ gauge boson $A_M^{U(1)_X}$, $P_0 = P_1 = 1$. For the $SO(5)_W$ gauge boson $A_M^{SO(5)_W}$, $P_0 = P_1 = P_{\mathbf{5}}^{SO(5)_W}$, where $P_{\mathbf{5}}^{SO(5)_W} = {\rm diag}(I_4, -I_1)$. The orbifold BCs of the $SO(5)_W$ symmetry break $SO(5)_W$ to $SO(4)_W \simeq SU(2)_L \times SU(2)_R$. W, Z bosons and γ (photon) are zero modes in the $SO(5)_W \times U(1)_X$ of 4 dimensional (4D) gauge bosons, whereas the 4D Higgs boson is a zero mode in the $SO(5)_W/SO(4)_W$ part of the 5th dimensional gauge boson. In the GHU model, extra neutral gauge bosons Z' correspond to the KK photons $\gamma^{(n)}$, the KK Z bosons $Z^{(n)}$, and the KK Z_R bosons $Z_R^{(n)}$ $(n \geq 1)$, where the γ, and Z, Z_R bosons are the mass eigenstates of the electromagnetic (EM) $U(1)_{\rm EM}$ neutral gauge bosons of $SU(2)_L$, $SU(2)_R$, and $U(1)_X$. Extra charged gauge bosons W' correspond to the KK W boson $W^{\pm(n)}$ $(n \geq 1)$ and the KK W_R bosons $W_R^{\pm(n)}$ $(n \geq 1)$.

The SM lepton multiples are identified with the zero modes of the lepton multiplets $\Psi^\alpha_{(\mathbf{1},\mathbf{4})}$ $(\alpha = 1, 2, 3)$ in the bulk, where the subscript of $\Psi^\alpha_{(\mathbf{1},\mathbf{4})}$ stands for the representations of $SU(3)_C \times SO(5)_W$. The bulk fields $\Psi^\alpha_{(\mathbf{1},\mathbf{4})}$ obey the following BCs:

$$\Psi^\alpha_{(\mathbf{1},\mathbf{4})}(x, y_j - y) = -P_{\mathbf{4}}^{SO(5)_W} \gamma^5 \Psi^\alpha_{(\mathbf{1},\mathbf{4})}(x, y_j + y), \tag{2.4}$$

where $P_{\mathbf{4}}^{SO(5)_W} = {\rm diag}(I_2, -I_2)$. From the BCs in Eq. (2.4), the left-handed Weyl fermion in $(\mathbf{2}, \mathbf{1})$ of $SU(2)_L \times SU(2)_R$ and the right-handed Weyl fermion in $(\mathbf{1}, \mathbf{2})$ of $SU(2)_L \times SU(2)_R$ have zero mode. Note that fermions in $(\mathbf{1}, \mathbf{1})(0)$ of $SU(3)_C \times SO(5)_W \times U(1)_X$ are also introduced as the brane fermions on the UV brane to reproduce tiny neutrino masses via the seesaw mechanism in the GHU model [27].

The brane scalar field in $\mathbf{4}$ of $SO(5)_W$ is introduced to realize the EW symmetry $SU(2)_L \times U(1)_Y$ at the EW scale. A spinor $\mathbf{4}$ of $SO(5)_W$ is decomposed into $(\mathbf{2}, \mathbf{1}) \oplus (\mathbf{1}, \mathbf{2})$ of $SO(4)_W \simeq SU(2)_L \times SU(2)_R$. We assume that the brane scalar develops a nonvanishing vacuum expectation value (VEV), which reduces the symmetry $SO(4)_W \times U(1)_X$ to the EW gauge symmetry $SU(2)_L \times U(1)_Y$, and the VEV of the brane scalar is much larger than $m_{\rm KK}$ to ensure that the orbifold BCs for the 4D components of the $SU(2)_R \times U(1)_X/U(1)_Y$ gauge fields become effectively Dirichlet conditions at the UV brane [25].

The $U(1)_Y$ gauge boson is realized as a linear combination of $U(1)_R (\subset SU(2)_R)$ and $U(1)_X$ gauge bosons. The $U(1)_Y$ gauge field B_M^Y is given in terms of the $SU(2)_R$ gauge fields $A_M^{a_R}$ $(a_R = 1_R, 2_R, 3_R)$ and the $U(1)_X$ gauge field B_M by $B_M^Y = \sin\phi A_M^{3_R} + \cos\phi B_M$. Here the mixing angle ϕ between $U(1)_R$ and $U(1)_X$ is given by $\cos\phi = g_A/\sqrt{g_A^2 + g_B^2}$ and $\sin\phi = g_B/\sqrt{g_A^2 + g_B^2}$, where g_A and g_B are gauge coupling constants in $SO(5)_W$ and $U(1)_X$, respectively. The 4D $SU(2)_L$ gauge coupling constant is given by $g_w = g_A/\sqrt{L}$. The 5 dimensional (5D) gauge coupling constant $g_Y^{\rm 5D}$ of $U(1)_Y$ and the 4D bare Weinberg angle at the tree level, θ_W^0, are given by

$$g_Y^{\rm 5D} = \frac{g_A g_B}{\sqrt{g_A^2 + g_B^2}}, \qquad \sin\theta_W^0 = \frac{\sin\phi}{\sqrt{1 + \sin^2\phi}}. \tag{2.5}$$

The 4D Higgs boson $\phi_H(x)$ is the zero mode contained in the $A_z = (kz)^{-1} A_y$ component:

$$A_z^{(j5)}(x, z) = \frac{1}{\sqrt{k}} \phi_j(x) u_H(z) + \cdots, \qquad u_H(z) = \sqrt{\frac{2}{z_L^2 - 1}}\, z,$$
$$\phi_H(x) = \frac{1}{\sqrt{2}} \begin{pmatrix} \phi_2 + i\phi_1 \\ \phi_4 - i\phi_3 \end{pmatrix}. \tag{2.6}$$

We take $\langle\phi_1\rangle, \langle\phi_2\rangle, \langle\phi_3\rangle = 0$ and $\langle\phi_4\rangle \neq 0$, which is related to the AB phase θ_H in the fifth dimension by $\langle\phi_4\rangle = \theta_H f_H$, where $f_H = 2 g_w^{-1} k^{1/2} L^{-1/2} (z_L^2 - 1)^{-1/2}$.

We will give a part of the bulk action below, where the full action is given in Ref. [22]. The action of each gauge field, $A_M^{SO(5)_W}$ or $A_M^{U(1)_X}$, is given in the form

$$S_{\rm bulk}^{\rm EW\ gauge} = \int d^5x \sqrt{-\det G} \left[-{\rm tr}\left(\frac{1}{4} F^{MN} F_{MN} + \frac{1}{2\xi} (f_{\rm gf})^2 + \mathcal{L}_{\rm gh} \right) \right], \tag{2.7}$$

where $\sqrt{-\det G} = 1/kz^5$, $z = e^{ky}$, tr is a trace over all group generators for each group, and F_{MN} is a field strength defined by $F_{MN} \coloneqq \partial_M A_N - \partial_N A_M - ig[A_M, A_N]$ with each 5D gauge coupling constant g. The second and third terms in Eq. (2.7) are the gauge fixing term and the ghost term given in Ref. [22], respectively. The action for the lepton sector in the bulk is given by

$$S_{\rm bulk}^{\rm lepton} = \int d^5x \sqrt{-\det G} \sum_{\alpha=1}^{3} \overline{\Psi^\alpha_{(\mathbf{1},\mathbf{4})}} \left[\gamma^A e_A{}^M \left(D_M + \frac{1}{8} \omega_{MBC} [\gamma^B, \gamma^C] \right) - c_L^\alpha \sigma'(y) \right] \Psi^\alpha_{(\mathbf{1},\mathbf{4})}, \tag{2.8}$$

where $\overline{\Psi^{\alpha}_{(\mathbf{1},\mathbf{4})}} = i\Psi^{\alpha}_{(\mathbf{1},\mathbf{4})}{}^{\dagger}\gamma^0$, $\sigma'(y) \coloneqq d\sigma(y)/dy$ and $\sigma'(y) = k$ for $0 < y < L$. Each lepton multiplet $\Psi^{\alpha}_{(\mathbf{1},\mathbf{4})}(x, y)$ has a bulk mass parameter c^{α}_L ($\alpha = 1, 2, 3$).

III. PARAMETER SETS

To evaluate cross sections and other observable quantities in W and Z boson pair production processes $e^-e^+ \to W^-W^+$ and $e^-e^+ \to ZZ$ at tree level in the GHU model, we need to know the masses, decay widths, and coupling constants of the gauge bosons, and the leptons. Parameters of the model are determined in the steps described in Refs. [53,57].

We present several parameter sets of the coupling constants of the leptons, which are necessary for the present analysis, where we omit quantities such as the mass and the decay width of $Z^{(1)}$ boson in the GHU model shown in Ref. [57]. In Sec. II, we gave only the 5D Lagrangian of the GHU model, but in the analysis, we use a 4D effective theory with KK mode expansion of the 5th dimension. By solving the equations of motions derived from the BCs of each 5D multiplet, we can obtain the mass spectra of 4D modes for each 5D field. Once mass spectra of a field are known, wave functions of the zero mode and the KK modes of the field can be determined by substituting mass spectra into the mode function of the field. Furthermore, coupling constants can be obtained by performing overlap integrals of the wave functions of the corresponding fields. For more details, see Ref. [57].

We will describe the steps to fix parameter sets in the GHU model, where we will show parameter sets for leptons, the gauge bosons, and the Higgs boson.

(1) We pick the values of θ_H and $m_{\mathrm{KK}} = \pi k(z_L - 1)^{-1}$. From the constraints on θ_H and m_{KK} from the LHC-Run 2 results in the GHU model [55], we only consider parameters satisfying $\theta_H \leq 0.10$ and $m_{\mathrm{KK}} \geq 13$ TeV.

(2) k is determined in order for the Z boson mass m_Z to be reproduced, which fixes the warped factor z_L as well. (For the mass formula of Z boson, see Ref. [22].)

(3) The bare Weinberg angle θ^0_W in the GHU model is given in Eq. (2.5). For each value of θ_H, the value of θ^0_W is determined self-consistently to fit the observed forward-backward asymmetry at Z pole as in Ref. [57].

The parameter sets of $(\theta_H, m_{\mathrm{KK}})$, named $A_{\pm}$,$B_{\pm}$, and $C_{\pm}$, used in this analysis are summarized in Table I, where the subscripts denote the sign of the bulk masses of the leptons. For example, A_+ denotes the case where the bulk mass of the lepton is positive and A_- denotes the case where the bulk mass of the lepton is negative.

(4) With given $\sin\theta^0_W$, wave functions of the gauge bosons are fixed. Masses and widths of $\gamma^{(1)}$ is listed for each parameter set in Table I, and those of $Z^{(1)}$, $Z^{(1)}_R$, W, $W^{(1)}$, $W^{(1)}_R$ bosons are listed for each parameter set in Table IV in Ref. [57].

(5) The bulk masses of the leptons c^{α}_L in Eq. (2.8) are determined so as to reproduce the masses of charged leptons, as the same in Ref. [57]. The bulk masses and the brane interaction parameters of the leptons are listed in Table V in Ref. [57].

(6) With given the bulk masses and the brane interaction parameters, wave functions of fermions are fixed.

(7) The mass of the Higgs boson can be obtained from the effective potential of the Higgs boson [52]. The mass of the Higgs boson is determined by adjusting the bulk mass of the dark fermions so that the mass of the Higgs boson is $m_h = 125.25 \pm 0.17$ GeV [12].

Next, coupling constants of the gauge bosons and the leptons are obtained from the five-dimensional gauge interaction terms by substituting the wave functions of gauge bosons and fermions and integrating over the fifth-dimensional coordinate [89,91,92]. The coupling constants of the gauge bosons to the leptons are obtained by performing overlap integrals of the wave functions in the fifth dimension of gauge bosons and leptons. Coupling constants of $\gamma^{(1)}$ to electron are listed in Table II. Coupling constants of gauge bosons to leptons are listed in Table VII in Ref. [57] for W boson to leptons Tables VII and VIII in

TABLE I. The name of the parameter set and the corresponding z_L, k, and $\sin^2\theta^0_W$ for each θ_H and m_{KK} are listed. In the SM, $\sin^2\theta_W(\overline{\mathrm{MS}}) = 0.23122 \pm 0.00004$ at Z pole [12]. The column "Name" denotes each parameter set. The subscripts of $A_{\pm}$, $B_{\pm}$, $C_{\pm}$ denote the sign of the bulk masses of the leptons. For example, A_+ denotes the case where the bulk mass of the lepton is positive and A_- denotes the case where the bulk mass of the lepton is negative. The names of the parameter sets are the same as those in Ref. [57].

Name	θ_H [rad]	m_{KK} [TeV]	z_L	k [GeV]	$m_{\gamma^{(1)}}$ [TeV]	$\Gamma_{\gamma^{(1)}}$ [TeV]	$m_{\nu^{(1)}}$ [TeV]	$m_{e^{(1)}}$ [TeV]	$\sin^2\theta^0_W$
A_-	0.10	13.00	3.865×10^{11}	1.599×10^{15}	10.198	3.252	13.039	13.039	0.2306
A_+	0.10	13.00	4.029×10^{11}	1.667×10^{15}	10.198	3.256	13.034	13.034	0.2318
B_-	0.07	19.00	1.420×10^{12}	8.589×10^{15}	14.887	4.951	18.852	18.852	0.2309
B_+	0.07	19.00	1.452×10^{12}	8.779×10^{15}	14.887	4.951	18.848	18.848	0.2315
C_-	0.05	25.00	5.546×10^{10}	4.413×10^{14}	19.649	5.862	25.528	25.528	0.2310
C_+	0.05	25.00	5.600×10^{10}	4.456×10^{14}	19.649	5.864	25.527	25.527	0.2313

TABLE II. Coupling constants of $\gamma^{(1)}$ boson to electrons and Z boson to electron and 1st KK electron in units of $g_w = e/\sin\theta_W^0$ are listed. When the value is less than 10^{-5}, we write 0.

Name	$g^L_{\gamma^{(1)}ee}$	$g^R_{\gamma^{(1)}ee}$	$g^L_{Zee^{(1)}}$	$g^R_{Zee^{(1)}}$
A_-	−2.75873	+0.10788	−0.01346	0
A_+	+0.10727	−2.54746	−0.01347	0
B_-	−2.81496	+0.10455	−0.00951	0
B_+	+0.10464	−2.81951	−0.00951	0
C_-	−2.57731	+0.11144	−0.00664	0
C_+	+0.11149	−2.67947	−0.00665	0

Ref. [57] for Z boson to neutrinos and charged leptons. MeV scale neutrino masses and coupling constants of W boson to electron are listed in Table III, where MeV neutrinos appear only when the bulk mass of the lepton is positive. The coupling constants of neutral gauge bosons to W boson are obtained by performing overlap integrals of the wave functions in the fifth dimension of triple gauge bosons. Coupling constants of neutral gauge bosons to W boson pair are listed in Table IV.

IV. CROSS SECTION

In this section, we give the formulas necessary to calculate observables of the $e^-e^+ \to W^-W^+$ and $e^-e^+ \to ZZ$ processes. In the SM, the cross sections of the $e^-e^+ \to W^-W^+$ and $e^-e^+ \to ZZ$ processes are calculated in e.g., Refs. [93–96]. We can use *Mathematica* and its package FeynCalc [97–99] in this section for computational checks, such as the contractions of the square of the amplitude.

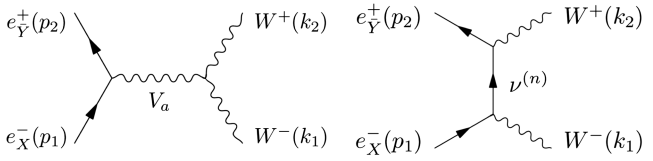

FIG. 1. The Feynman diagrams for the s-channel and t-channel contributions to the $e^-e^+ \to W^-W^+$ process are shown. For the s-channel contribution, V_a stands for γ, Z in the SM and for $\gamma^{(n)}$, $Z^{(n)}$, $Z_R^{(n)}$ $(n = 1, 2, \ldots)$ in the GHU model. For the t-channel contribution, $\nu^{(n)}$ stands for ν_e in the SM and for $\nu_e^{(n)}$ (and $\nu_{e2}^{(n)}$) in the GHU model.

A. Cross section of $e^-e^+ \to W^-W^+$

1. Amplitude

We consider the W^-W^+ production processes:

$$e^-_X(p_1)e^+_Y(p_2) \longrightarrow W^-(k_1)W^+(k_2), \tag{4.1}$$

where $X, Y = L, R$; p_1 and p_2 are the momenta of the initial states of electron and positron; k_1 and k_2 are the momenta of the final states of W^- and W^+ bosons. This is shown in Fig. 1. For massive bosons $W^\pm$ and massless electrons $e^\pm$, in the center-of-mass frame, we use the following basis:

$$\begin{aligned} p_1^\mu &= \frac{\sqrt{s}}{2}(1,0,0,+1), \qquad p_2^\mu = \frac{\sqrt{s}}{2}(1,0,0,-1), \\ k_1^\mu &= \frac{\sqrt{s}}{2}(1,+\beta_W\sin\theta,0,+\beta_W\cos\theta), \\ k_2^\mu &= \frac{\sqrt{s}}{2}(1,-\beta_W\sin\theta,0,-\beta_W\cos\theta), \end{aligned} \tag{4.2}$$

TABLE III. MeV scale neutrino masses and coupling constants of W boson to electron are listed in units of MeV and $g_w/\sqrt{2}$, respectively. There are no such neutrinos for negative lepton bulk masses. $\Delta m_{\nu_{\rm MeV}} := m_{\nu_{\rm MeV}} - m_{\nu'_{\rm MeV}} \simeq 4.0\times10^{-7}$ MeV, 8.2×10^{-7} MeV, 1.6×10^{-6} MeV for A_+, B_+, C_+, respectively.

Name	$m_{\nu_{\rm MeV}}$ [MeV]	$m_{\nu'_{\rm MeV}}$ [MeV]	$g^L_{We\nu_{\rm MeV}e}$	$g^R_{We\nu_{\rm MeV}e}$	$g^L_{We\nu'_{\rm MeV}e}$	$g^R_{We\nu'_{\rm MeV}e}$
A_+	9.735	9.735	−0.03534	−0.00177	+0.03534	+0.00177
B_+	13.904	13.904	−0.02474	−0.00087	+0.02474	+0.00087
C_+	19.464	19.464	−0.01768	−0.00044	+0.01768	+0.00044

TABLE IV. Coupling constants of neutral gauge bosons to W boson in units of g_w are listed. In the SM and the GHU, $g_{\gamma WW} = e$, and $g_{\gamma WW}/g_w = 0.48085$. In the SM, $g_{ZWW}/g_w = \cos\theta_W = 0.87680$.

Name	$g_{\gamma^{(1)}WW}$ [GeV]	g_{ZWW} [GeV]	$g_{Z^{(1)}WW}$ [GeV]	$g_{Z_R^{(1)}WW}$ [GeV]
A_-	−0.00029	+0.87715	−0.00019	+0.00027
A_+	−0.00029	+0.87647	−0.00019	+0.00027
B_-	−0.00014	+0.87698	−0.00009	+0.00013
B_+	−0.00014	+0.87664	−0.00009	+0.00013
C_-	−0.00008	+0.87693	−0.00005	+0.00007
C_+	−0.00008	+0.87676	−0.00005	+0.00007

where $\beta_W \coloneqq \sqrt{1-\frac{4m_W^2}{s}}$. The Mandelstam variables are defined as

$$\begin{aligned} s &\coloneqq (p_1+p_2)^2 = (k_1+k_2)^2, \\ t &\coloneqq (p_1-k_1)^2 = (p_2-k_2)^2 = m_W^2 - \frac{s}{2}(1-\beta_W\cos\theta), \\ u &\coloneqq (p_1-k_2)^2 = (p_2-k_1)^2 = m_W^2 - \frac{s}{2}(1+\beta_W\cos\theta), \end{aligned} \tag{4.3}$$

where $s+t+u = 2m_W^2$.

The contributions to the $e^-e^+ \to W^-W^+$ process come from s-channel and t-channel. The s-channel amplitude is given by

$$\begin{aligned} \mathcal{M}_{sXY}^{WW} &= \bar{v}(p_2)\gamma_\rho P_Y P_X u(p_1) V^{\mu\nu\rho}(-k_1,-k_2,k_1+k_2) \\ &\quad \times \epsilon_\mu^*(k_1)\epsilon_\nu^*(k_2)\sum_a g_{V_a ee}^X g_{V_a WW} \\ &\quad \times \frac{1}{(s-m_{V_a}^2)+im_{V_a}\Gamma_{V_a}} \\ &\eqqcolon J_{sXY}^{\mu\nu}\epsilon_\mu^*(k_1)\epsilon_\nu^*(k_2), \end{aligned} \tag{4.4}$$

where $V^{\alpha\beta\gamma}(q,k_-,k_+) \coloneqq [(q-k_-)^\gamma g^{\alpha\beta} + (k_- - k_+)^\alpha g^{\beta\gamma} + (k_+ - q)^\beta g^{\gamma\alpha}]$, $q^\mu = (p_1+p_2)^\mu = (k_1+k_2)^\mu$, $g_{V_a ff}^{L/R}$ are the left-(right-)handed couplings of f to V_a. $g_{V_a WW}$ is the coupling constant of $V_a - W - W$, where m_{V_a} and Γ_{V_a} are mass and total decay width of V_a. $q^\mu = (p_1+p_2)^\mu = (k_2+k_1)^\mu$. The $J_{sXY}^{\mu\nu}$ can be written as

$$J_{sXY}^{\mu\nu} = \begin{cases} A_{sX}^{WW}\bar{v}(p_2)\gamma_\rho P_X u(p_1) V^{\mu\nu\rho}(-k_1,-k_2,k_1+k_2) & \text{for } X = Y \\ 0 & \text{for } X \neq Y \end{cases}, \tag{4.5}$$

where

$$A_{sX}^{WW} \coloneqq \sum_a g_{V_a ee}^X g_{V_a WW}\frac{1}{(s-m_{V_a}^2)+im_{V_a}\Gamma_{V_a}}. \tag{4.6}$$

The t-channel amplitude is given by

$$\begin{aligned} \mathcal{M}_{tXY}^{WW} &= -\epsilon_\mu^*(k_1)\epsilon_\nu^*(k_2)\bar{v}(p_2)P_Y\gamma^\nu\left\{\sum_n g_{We\nu^{(n)}}^X g_{We\nu^{(n)}}^Y \right. \\ &\quad \left. \times \frac{(\not{p}_1 - \not{k}_1) + m_{\nu^{(n)}}}{(t-m_{\nu^{(n)}}^2)}\right\}\gamma^\mu P_X u(p_1) \\ &\eqqcolon J_{tXY}^{\mu\nu}\epsilon_\mu^*(k_1)\epsilon_\nu^*(k_2). \end{aligned} \tag{4.7}$$

The $J_{tXY}^{\mu\nu}$ can be written as

$$J_{tXY}^{\mu\nu} = \begin{cases} -A_{tX}^{WW}\bar{v}(p_2)\gamma^\nu(\not{p}_1 - \not{k}_1)\gamma^\mu P_X u(p_1) & \text{for } X = Y \\ -B_t^{WW}\bar{v}(p_2)\gamma^\nu\gamma^\mu P_X u(p_1) & \text{for } X \neq Y \end{cases}, \tag{4.8}$$

where

$$A_{tX}^{WW} \coloneqq \sum_n \frac{(g_{We\nu^{(n)}}^X)^2}{t-m_{\nu^{(n)}}^2}, \qquad B_t^{WW} \coloneqq \sum_n \frac{g_{We\nu^{(n)}}^L g_{We\nu^{(n)}}^R m_{\nu^{(n)}}}{t-m_{\nu^{(n)}}^2}. \tag{4.9}$$

2. Squared amplitude

The squared amplitude of the $e_X^- e_Y^+ \to W^-W^+$ process is given by

$$\begin{aligned} |\mathcal{M}_{XY}^{WW}|^2 &= |\mathcal{M}_{sXY}^{WW} + \mathcal{M}_{tXY}^{WW}|^2 \\ &= |\mathcal{M}_{sXY}^{WW}|^2 + |\mathcal{M}_{tXY}^{WW}|^2 + \mathcal{M}_{sXY}^{WW}\mathcal{M}_{tXY}^{WW\dagger} \\ &\quad + \mathcal{M}_{sXY}^{WW\dagger}\mathcal{M}_{tXY}^{WW}. \end{aligned} \tag{4.10}$$

The third and forth terms stand for the interference terms between s- and t-channel.

First, from Eq. (4.4), the s-channel contribution $|\mathcal{M}_{sXY}^{WW}|^2$ is given by

$$\begin{aligned} |\mathcal{M}_{sXY}^{WW}|^2 &= \sum_{\text{spins}} \epsilon_\mu^*(k_1)\epsilon_\nu^*(k_2)\epsilon_{\mu'}(k_1)\epsilon_{\nu'}(k_2) J_{sXY}^{\mu\nu}\bar{J}_{sXY}^{\mu'\nu'} \\ &= \left(-g_{\mu\mu'} + \frac{k_{1\mu}k_{1\mu'}}{k_1^2}\right)\left(-g_{\nu\nu'} + \frac{k_{2\nu}k_{2\nu'}}{k_2^2}\right) \\ &\quad \times \sum_{\text{spins}} J_{sXY}^{\mu\nu}\bar{J}_{sXY}^{\mu'\nu'}. \end{aligned} \tag{4.11}$$

Substituting Eq. (4.5) into Eq. (4.11), we find

$$|\mathcal{M}_{sXY}^{WW}|^2 = \begin{cases} 4s^2|A_{sX}^{WW}|^2 A(s,t,u) & \text{for } X = Y \\ 0 & \text{for } X \neq Y \end{cases}, \tag{4.12}$$

where

$$A(s,t,u) \coloneqq \left(\frac{tu}{m_W^4} - 1\right)\left(\frac{1}{4} - \frac{m_W^2}{s} + 3\frac{m_W^4}{s^2}\right) + \frac{s}{m_W^2} - 4. \tag{4.13}$$

Second, from Eq. (4.7) the t-channel contribution $|\mathcal{M}_{tXY}^{WW}|^2$ is given by

$$|\mathcal{M}^{WW}_{tXY}|^2 = \sum_{\text{spins}} \epsilon^*_\mu(k_1)\epsilon^*_\nu(k_2)\epsilon_{\mu'}(k_1)\epsilon_{\nu'}(k_2) J^{\mu\nu}_{tXY}\bar{J}^{\mu'\nu'}_{tXY}$$
$$= \left(-g_{\mu\mu'} + \frac{k_{1\mu}k_{1\mu'}}{k_1^2}\right)\left(-g_{\nu\nu'} + \frac{k_{2\nu}k_{2\nu'}}{k_2^2}\right)\sum_{\text{spins}} J^{\mu\nu}_{tXY}\bar{J}^{\mu'\nu'}_{tXY}. \tag{4.14}$$

Substituting Eq. (4.8) into Eq. (4.14), we find

$$|\mathcal{M}^{WW}_{tXY}|^2 = \begin{cases} |tA^{WW}_{tX}|^2 \cdot 4E(s,t,u) & \text{for } X = Y \\ |tB^{WW}_t|^2 4\left[\frac{2m_W^2}{t^2}\left(\frac{tu}{m_W^4} - 1\right) + \frac{2s}{t^2} + \frac{s}{2m_W^4}\right] & \text{for } X \neq Y \end{cases}, \tag{4.15}$$

where

$$E(s,t,u) \coloneqq \left(\frac{tu}{m_W^4} - 1\right)\left(\frac{1}{4} + \frac{m_W^4}{t^2}\right) + \frac{s}{m_W^2}. \tag{4.16}$$

Finally, we consider the interference terms in Eq. (4.10). Due to $\mathcal{M}_{sXY} = 0$ for $X \neq Y$,

$$\mathcal{M}_{sXY}\mathcal{M}^\dagger_{tXY} = \mathcal{M}^\dagger_{sXY}\mathcal{M}_{tXY} = 0. \tag{4.17}$$

Therefore, the nonzero values of the interference terms are given by

$$\mathcal{M}^{WW}_{sXX}\mathcal{M}^{WW\dagger}_{tXX} = \sum_{\text{spins}} \epsilon^*_\mu(k_1)\epsilon^*_\nu(k_2)\epsilon_{\mu'}(k_1)\epsilon_{\nu'}(k_2) J^{\mu\nu}_{sXX}\bar{J}^{\mu'\nu'}_{tXX}$$
$$= \left(-g_{\mu\mu'} + \frac{k_{+\mu}k_{+\mu'}}{k_+^2}\right)\left(-g_{\nu\nu'} + \frac{k_{-\nu}k_{-\nu'}}{k_-^2}\right) \times \sum_{\text{spins}} J^{\mu\nu}_{sXX}\bar{J}^{\mu'\nu'}_{tXX}. \tag{4.18}$$

Substituting Eqs. (4.5) and (4.8) into Eq. (4.18), we find

$$\mathcal{M}^{WW}_{sXY}\mathcal{M}^{WW\dagger}_{tXY} = \begin{cases} A^{WW}_{sX}A^{WW*}_{tX} \cdot 4stI(s,t,u) & \text{for } X = Y \\ 0 & \text{for } X \neq Y \end{cases}, \tag{4.19}$$

where

$$I(s,t,u) = \left(\frac{tu}{m_W^4} - 1\right)\left(\frac{1}{4} - \frac{m_W^2}{2s} - \frac{m_W^4}{st}\right) + \frac{s}{m_W^2} - 2 + 2\frac{m_W^2}{t}. \tag{4.20}$$

From Eqs. (4.12), (4.15), and (4.19), the total amplitude of $e^-_X e^+_{\bar{Y}} \to W^-W^+$ for $X = Y$ given by

$$|\mathcal{M}^{WW}_{XY}|^2 = 4s^2|A^{WW}_{sX}|^2 A(s,t,u) + 4t^2|A^{WW}_{tX}|^2 E(s,t,u) + 4st(A^{WW}_{sX}A^{WW*}_{tX} + A^{WW*}_{sX}A^{WW}_{tX})I(s,t,u), \tag{4.21}$$

where $A(s,t,u)$, $E(s,t,u)$, and $I(s,t,u)$ are defined in Eqs. (4.13), (4.16), and (4.20), respectively. The total amplitude of $e^-_X e^+_{\bar{Y}} \to W^-W^+$ for $X \neq Y$ given by

$$|\mathcal{M}^{WW}_{XY}|^2 = |tB^{WW}_t|^2\left[\frac{4s}{t^2} + \frac{s}{m_W^4} + \frac{4}{m_W^2}\left(\frac{u}{t} - \frac{m_W^4}{t^2}\right)\right]. \tag{4.22}$$

3. Cross section

For the $e^-_X e^+_{\bar{Y}} \to W^-W^+$ process, the cross section of the initial states of the polarized electron and positron is given by

$$\frac{d\sigma^{WW}}{d\cos\theta}(P_{e^-}, P_{e^+}, \cos\theta) = \frac{1}{4}\Big\{(1 - P_{e^-})(1 + P_{e^+})\frac{d\sigma^{WW}_{LL}}{d\cos\theta} + (1 + P_{e^-})(1 - P_{e^+})\frac{d\sigma^{WW}_{RR}}{d\cos\theta} + (1 - P_{e^-})(1 - P_{e^+})\frac{d\sigma^{WW}_{LR}}{d\cos\theta} + (1 + P_{e^-})(1 + P_{e^+})\frac{d\sigma^{WW}_{RL}}{d\cos\theta}\Big\}, \tag{4.23}$$

where P_{e^-} and P_{e^+} are the initial polarizations of the electron and positron

$$\frac{d\sigma^{WW}_{XY}}{d\cos\theta}(\cos\theta) \coloneqq \frac{d\sigma}{d\cos\theta}\left(e^-_X e^+_{\bar{Y}} \to W^-W^+\right) = \frac{\beta_W}{32\pi s}|\mathcal{M}^{WW}_{XY}|^2, \tag{4.24}$$

where $\mathcal{M}^{WW}_{XY}$ are given in Eqs. (4.21) and (4.22)

The total cross section of the $e^-e^+ \to W^-W^+$ process with the initial polarizations can be defined by integrating the differential cross section in Eq. (4.23) with the angle θ

$$\sigma^{WW}(P_{e^-}, P_{e^+}) \coloneqq \int_{-1}^{1} \frac{d\sigma^{WW}}{d\cos\theta}\left(P_{e^-}, P_{e^+}, \cos\theta\right) d\cos\theta, \tag{4.25}$$

where the minimum and maximal values of $\cos\theta$ are determined by each detector and we cannot use a date near $\cos\theta \simeq \pm 1$. The total cross section of $e^-e^+ \to W^-W^+$ is given by

$$\begin{aligned}\sigma^{WW}(P_{e^-}, P_{e^+}) = &\frac{1}{4}(1-P_{e^-})(1+P_{e^+})\sigma^{WW}_{LL} \\ &+\frac{1}{4}(1+P_{e^-})(1-P_{e^+})\sigma^{WW}_{RR} \\ &+\frac{1}{4}(1-P_{e^-})(1-P_{e^+})\sigma^{WW}_{LR} \\ &+\frac{1}{4}(1+P_{e^-})(1+P_{e^+})\sigma^{WW}_{RL}, \end{aligned} \tag{4.26}$$

where

$$\sigma^{WW}_{XY} \coloneqq \int_{-1}^{1} \frac{d\sigma^{WW}_{XY}}{d\cos\theta}(\cos\theta) d\cos\theta, \tag{4.27}$$

where $X = L, R$; $d\sigma^{WW}_{XY}/d\cos\theta$ are given in Eq. (4.24).

The statistical error of the cross section $\sigma^{WW}(P_{e^-}, P_{e^+})$ is given by

$$\begin{aligned}\Delta\sigma^{WW}(P_{e^-}, P_{e^+}) &= \frac{\sigma^{WW}(P_{e^-}, P_{e^+})}{\sqrt{N^{WW}}}, \\ N^{WW} &= L_{\rm int} \cdot \sigma^{WW}(P_{e^-}, P_{e^+}), \end{aligned} \tag{4.28}$$

where $L_{\rm int}$ is an integrated luminosity, and N^{WW} is the number of events for the $e^-e^+ \to W^-W^+$ process. Note that the W boson cannot be observed directly, so we need to choose the decay modes of the W boson, and then the available number of events must be N^{WW} multiplied by the branching ratio of each selected decay mode. The amount of the deviation of the cross section of the $e^-e^+ \to W^-W^+$ process from the SM in the GHU model is given by

$$\Delta^{WW}_{\sigma}(P_{e^-}, P_{e^+}) \coloneqq \frac{[\sigma^{WW}(P_{e^-}, P_{e^+})]_{\rm GHU}}{[\sigma^{WW}(P_{e^-}, P_{e^+})]_{\rm SM}} - 1, \tag{4.29}$$

where $[\sigma^{WW}(P_{e^-}, P_{e^+})]_{\rm GHU}$ and $[\sigma^{WW}(P_{e^-}, P_{e^+})]_{\rm SM}$ stand for the cross sections of the $e^-e^+ \to W^-W^+$ process in the SM and the GHU model, respectively. The same notation is used for other cases in the followings.

4. Left-right asymmetry

We define an observable left-right asymmetry [53,56,81,82,100] of the $e^-e^+ \to W^-W^+$ process as

$$A^{WW}_{LR}(P_{e^-}, P_{e^+}) \coloneqq \frac{\sigma^{WW}(P_{e^-}, P_{e^+}) - \sigma^{WW}(-P_{e^-}, -P_{e^+})}{\sigma^{WW}(P_{e^-}, P_{e^+}) + \sigma^{WW}(-P_{e^-}, -P_{e^+})} \tag{4.30}$$

for $P_{e^-} < 0$ and $|P_{e^-}| > |P_{e^+}|$.

The statistical error of the left-right asymmetry is given by

$$\Delta A^{WW}_{LR}(P_{e^-}, P_{e^+}) = 2\frac{\sqrt{N^{WW}_L N^{WW}_R}(\sqrt{N^{WW}_L} + \sqrt{N^{WW}_R})}{(N^{WW}_L + N^{WW}_R)^2}, \tag{4.31}$$

where $N^{WW}_L = L_{\rm int}\sigma^{WW}(P_{e^-}, P_{e^+})$ and $N^{WW}_R = L_{\rm int}\sigma^{WW}(-P_{e^-}, -P_{e^+})$ are the numbers of the events for $P_{e^-} < 0$ and $|P_{e^-}| > |P_{e^+}|$. The amount of the deviation from the SM in Eq. (4.30) is characterized by

$$\Delta^{WW}_{A_{LR}}(P_{e^-}, P_{e^+}) \coloneqq \frac{[A^{WW}_{LR}(P_{e^-}, P_{e^+})]_{\rm GHU}}{[A^{WW}_{LR}(P_{e^-}, P_{e^+})]_{\rm SM}} - 1. \tag{4.32}$$

5. Asymptotic behavior

We consider the asymptotic behavior of $e^-e^+ \to W^-W^+$ for large s to confirm that the Goldstone boson equivalence theorem [86–88] is satisfied in the GHU model. From Eqs. (4.23), (4.24), and (4.26), very large cross section appears if the total squared amplitude of $|\mathcal{M}^{WW}_{XY}|^2$ contain $O(s^2)$ terms. The $O(s)$ terms of the squared amplitude do not break unitarity because the Froissart bound [84,85] is satisfied. In this section we consider the $O(s^2)$ and $O(s)$ terms of the squared amplitude. In the SM, the $O(s)$ terms vanish.

The total amplitudes of $e^-_X e^+_Y \to W^-W^+$ are given in Eqs. (4.21) and (4.22). First, from Eqs. (4.6) and (4.9), the asymptotic behavior of A^{WW}_{sX}, A^{WW}_{tX}, and B^{WW}_t for large s is given by

$$\begin{aligned} sA^{WW}_{sX} &\sim \sum_a g^X_{V_a ee} g_{V_a WW}\left(1 + \frac{m^2_{V_a}}{s}\right), \\ tA^{WW}_{tX} &\sim \sum_n (g^X_{We\nu^{(n)}})^2\left(1 + \frac{m^2_{\nu^{(n)}}}{t}\right), \\ tB^{WW}_t &\sim \sum_n g^L_{We\nu^{(n)}} g^R_{We\nu^{(n)}} m_{\nu^{(n)}}\left(1 + \frac{m^2_{\nu^{(n)}}}{t}\right), \end{aligned} \tag{4.33}$$

where we ignore the decay width Γ_{V_a} for simplicity. Second, from Eqs. (4.13), (4.16), and (4.20), the asymptotic behavior of $A(s,t,u)$, $E(s,t,u)$, and $I(s,t,u)$ for large s is given by

$$\begin{aligned} 4A(s,t,u) &\sim \frac{tu}{m^4_W} - \frac{4tu}{sm^2_W} + \frac{4s}{m^2_W} \\ 4E(s,t,u) &\sim \frac{tu}{m^4_W} + \frac{4s}{m^2_W}, \\ 4I(s,t,u) &\sim \frac{tu}{m^4_W} - \frac{2tu}{sm^2_W} + \frac{4s}{m^2_W}. \end{aligned} \tag{4.34}$$

Substituting Eqs. (4.33) and (4.34) into Eq. (4.21), we find the asymptotic behavior of $|\mathcal{M}_{XY}^{WW}|^2$ for $X = Y$:

$$\begin{aligned}|\mathcal{M}_{XY}^{WW}|^2 \sim & \left(\sum_a g^X_{V_a ee} g_{V_a WW} + \sum_n \left(g^X_{We\nu^{(n)}}\right)^2\right) \\ & \times \left[\left(\sum_a g^X_{V_a ee} g_{V_a WW} + \sum_n \left(g^X_{We\nu^{(n)}}\right)^2\right) \right. \\ & \times \left(\frac{tu}{m_W^4} + \frac{4s}{m_W^2}\right) - 2\left\{\sum_b g^X_{V_b ee} g_{V_b WW} \right. \\ & \left. \left. - \sum_b g^X_{V_b ee} g_{V_b WW} \frac{m_{V_b}^2}{m_W^2}\right\} \frac{tu}{sm_W^2} \right. \\ & \left. + 2\left(\sum_m \left(g^X_{We\nu^{(m)}}\right)^2 \frac{m^2_{\nu^{(m)}}}{m_W^2}\right) \frac{u}{m_W^2}\right]. \end{aligned} \tag{4.35}$$

Substituting Eqs. (4.33) and (4.34) into Eq. (4.22), we find the asymptotic behavior of $|\mathcal{M}_{XY}^{WW}|^2$ for $X \neq Y$:

$$|\mathcal{M}_{XY}^{WW}|^2 \sim \left(\sum\nolimits_n g^L_{We\nu^{(n)}} g^R_{We\nu^{(n)}} \frac{m_{\nu^{(n)}}}{m_W}\right)^2 \frac{s}{m_W^2}. \tag{4.36}$$

Here we summarize the above results. From the asymptotic behavior of $|\mathcal{M}_{XY}^{WW}|^2$ for $X = Y$ in Eq. (4.35), $O(s^2)$ terms disappear when the following condition is satisfied:

$$\sum_a g^X_{V_a ee} g_{V_a WW} + \sum_n \left(g^X_{We\nu^{(n)}}\right)^2 = 0. \tag{4.37}$$

The $O(s)$ terms also disappear if this condition is satisfied. Next, from the asymptotic behavior of $|\mathcal{M}_{XY}^{WW}|^2$ for $X \neq Y$ in Eq. (4.36), $O(s)$ terms disappear when the following condition is satisfied:

$$\sum_n g^L_{We\nu^{(n)}} g^R_{We\nu^{(n)}} \frac{m_{\nu^{(n)}}}{m_W} = 0. \tag{4.38}$$

We check that the unitarity is preserved in the SM and the GHU below by using Eqs. (4.37) and (4.38). First, in the SM, $V_a = \gamma$, Z and $\nu^{(n)} = \nu_e$, relevant coupling constants are given by

$$\begin{aligned} & g^L_{\gamma ee} = g^R_{\gamma ee} = -e, \quad g_{\gamma WW} = e, \quad g_{ZWW} = g_w \cos\theta_W, \\ & g^L_{We\nu_e} = \frac{g_w}{\sqrt{2}}, \quad g^R_{We\nu_e} = 0, \\ & g^L_{Zee} = \frac{g_w}{\cos\theta_W}\left(-\frac{1}{2} + \sin^2\theta_W\right), \quad g^R_{Zee} = \frac{g_w}{\cos\theta_W}\sin^2\theta_W, \end{aligned} \tag{4.39}$$

where $g_w = e/\sin\theta_W$. Therefore, we find

$$\begin{aligned} & \sum_a g^L_{V_a ee} g_{V_a WW} = g^L_{\gamma ee} g_{\gamma WW} + g^L_{Ze} g_{ZWW} = -\frac{g_w^2}{2}, \\ & \sum_n \left(g^L_{We\nu^{(n)}}\right)^2 = \left(g^L_{We\nu}\right)^2 = \frac{g_w^2}{2}, \\ & \sum_a g^R_{V_a ee} g_{V_a WW} = g^R_{\gamma ee} g_{\gamma WW} + g^R_{Ze} g_{ZWW} = 0, \\ & \sum_n \left(g^R_{We\nu^{(n)}}\right)^2 = \left(g^R_{We\nu}\right)^2 = 0. \end{aligned} \tag{4.40}$$

Substituting the above SM gauge coupling constants into Eq. (4.37), the coefficients of the $O(s^2)$ and $O(s)$ terms of $\mathcal{M}_{LL}^{WW}$ and $\mathcal{M}_{RR}^{WW}$ vanish. Next, even when we take into account the non-zero neutrino mass $m_\nu \neq 0$, since $g^R_{We\nu} = 0$ in the SM, we find

$$\sum_n g^L_{We\nu^{(n)}} g^R_{We\nu^{(n)}} \frac{m_{\nu^{(n)}}}{m_W} = g^L_{We\nu} g^R_{We\nu} \frac{m_\nu}{m_W} = 0. \tag{4.41}$$

Therefore, the coefficients of the $O(s)$ terms of $\mathcal{M}_{LR}^{WW}$ and $\mathcal{M}_{RL}^{WW}$ vanish.

We consider the GHU model with the parameter set for $m_{\rm KK} = 13$ TeV, $\theta_H = 0.10$, and negative bulk masses of the leptons. For the GHU model, $V_a = \gamma, Z, \gamma^{(n)}, Z^{(n)}, Z_R^{(m)}$ $(n = 1, 2, \ldots)$ and $\nu^{(n)} = \nu_e, \nu_e^{(n)}$ $(n = 1, 2, \ldots)$, relevant coupling constants are given in Table V, where the following calculation of the sum of coupling constants adds up to a sufficiently large KK mode. We find

$$\begin{aligned} & \sum_a g^L_{V_a ee} g_{V_a WW} \simeq -0.49793312 g_w^2, \\ & \sum_n (g^L_{We\nu^{(n)}})^2 \simeq +0.49793310 g_w^2, \\ & \left|\sum_a g^R_{V_a ee} g_{V_a WW}\right| < 10^{-8} \times g_w^2, \\ & \left|\sum_n (g^R_{We\nu^{(n)}})^2\right| < 10^{-8} \times g_w^2. \end{aligned} \tag{4.42}$$

We numerically find

$$\begin{aligned} & \sum_a g^L_{V_a ee} g_{V_a WW} + \sum_n \left(g^L_{We\nu^{(n)}}\right)^2 \simeq -2 \times 10^{-8} g_w^2, \\ & \left|\sum_a g^R_{V_a ee} g_{V_a WW} + \sum_n \left(g^R_{We\nu^{(n)}}\right)^2\right| < 10^{-8} \times g_w^2. \end{aligned} \tag{4.43}$$

Therefore, the $O(s^2)$ and $O(s)$ terms of $\mathcal{M}_{LL}^{WW}$ and $\mathcal{M}_{RR}^{WW}$ are well suppressed. We also find

$$\left|\sum_n g^L_{We\nu^{(n)}} g^R_{We\nu^{(n)}} \frac{m_{\nu^{(n)}}}{m_W}\right| < 10^{-8} \times g_w^2. \tag{4.44}$$

TABLE V. Coupling constants of W bosons to neutral gauge bosons, electrons to neutral gauge bosons, W bosons to electron and zero mode,and KK neutrinos are shown up to $n = 4$ in the GHU model with the parameter set of $m_{\mathrm{KK}} = 13$ TeV and $\theta_H = 0.10$, and negative bulk masses of the leptons (A_-). The values of the coupling constants for neutral gauge bosons to W bosons and leptons are given in units of g_w. The values of the coupling constants for W boson to leptons are in units of $g_w/\sqrt{2}$. $g_w = e/\sin\theta_W^0$, $\sin^2\theta_W^0 = 0.2306$ (input). In the SM $\sin^2\theta_W(\overline{\mathrm{MS}}) = 0.23122 \pm 0.00004$ [12]. When the value is less than 10^{-8}, we write 0. When there is no corresponding coupling constant, we write the symbol $\cdots$ in that field.

Coupling	$n = 0$	$n = 1$	$n = 2$	$n = 3$	$n = 4$
$g_{\gamma^{(n)}WW}$	$+\sin\theta_W^0$	−0.00029313	−0.00001057	−0.00000185	+0.00000052
$g_{Z^{(n)}WW}$	+0.87715447	−0.00018818	+0.00000002	−0.00000679	−0.00000002
$g_{Z_R^{(n)}WW}$	$\cdots$	+0.00027271	+0.00000983	+0.00000163	+0.00000047
$g^L_{\gamma^{(n)}ee}$	$-\sin\theta_W^0$	−2.75873260	−1.08511541	−0.39362141	−0.23177025
$g^R_{\gamma^{(n)}ee}$	$-\sin\theta_W^0$	+0.10708192	−0.07393235	+0.06029203	−0.05236728
$g^L_{Z^{(n)}ee}$	−0.30576326	−1.76206116	−0.00643559	−0.69313977	−0.00209004
$g^R_{Z^{(n)}ee}$	+0.26291828	−0.05843186	−0.00396529	+0.04034314	+0.00296713
$g^L_{Z_R^{(n)}ee}$	$\cdots$	−1.04437969	−0.41581800	−0.14941965	−0.08774238
$g^R_{Z_R^{(n)}ee}$	$\cdots$	0	0	0	0
$g^L_{We\nu_e^{(n)}}$	+0.99764683	−0.01669268	−0.00001276	+0.00209568	−0.00000029
$g^R_{We\nu_e^{(n)}}$	0	0	0	0	0
$g^L_{We\nu_{e2}^{(n)}}$	$\cdots$	−0.01669268	−0.00001276	+0.00209568	−0.00000029
$g^R_{We\nu_{e2}^{(n)}}$	$\cdots$	0	0	0	0

TABLE VI. The values of the coupling summation are summarized for several sets of parameters $(m_{\mathrm{KK}}, \theta_H)$ with negative bulk masses of the leptons in the units of g_w^2. When the value is less than 10^{-8}, we write 0.

$(m_{\mathrm{KK}}, \theta_H)$	SM	(13 TeV, 0.10)	(25 TeV, 0.05)	(50 TeV, 0.025)	(100 TeV, 0.0125)
$\sum_a g^L_{V_aee} g_{V_aWW}$	−0.5	−0.49793312	−0.499484367	−0.49987087	−0.49996771
$\sum_n (g^L_{We\nu^{(n)}})^2$	+0.5	+0.49793310	+0.499448367	+0.49987087	+0.49996771
$\sum_a g^R_{V_aee} g_{V_aWW}$	0	0	0	0	0
$\sum_n (g^R_{We\nu^{(n)}})^2$	0	0	0	0	0
$\sum_n g^L_{We\nu^{(n)}} g^R_{We\nu^{(n)}} \frac{m_{\nu^{(n)}}}{m_W}$	0	0	0	0	0

The $O(s)$ term of $\mathcal{M}_{LR}^{WW}$ and $\mathcal{M}_{RL}^{WW}$ is sufficiently suppressed. Several other parameter sets are also summarized in Table VI.

Next, we consider the GHU model with the parameter set for $m_{\mathrm{KK}} = 13$ TeV, $\theta_H = 0.10$, and positive bulk masses of leptons. For the GHU model, $V_a = \gamma, Z, \gamma^{(n)}, Z^{(n)}, Z_R^{(m)}$ $(n = 1, 2, \ldots)$ and $\nu^{(n)} = \nu_e, \nu_e^{(n)}$ $(n = 1, 2, \ldots)$, relevant coupling constants are given in Table VII, where the following calculation of the sum of coupling constants adds up to a sufficiently large KK mode. We find

$$\sum_a g^L_{V_aee} g_{V_aWW} \simeq -0.50006646 g_w^2, \qquad \sum_n \left(g^L_{We\nu^{(n)}}\right)^2 \simeq +0.50006646 g_w^2,$$
$$\sum_a g^R_{V_aee} g_{V_aWW} \simeq -0.00028680 g_w^2, \qquad \sum_n \left(g^R_{We\nu^{(n)}}\right)^2 \simeq +0.00028680 g_w^2. \tag{4.45}$$

TABLE VII. Coupling constants of W bosons to neutral gauge bosons, electrons to neutral gauge bosons, W bosons to electron and zero mode, and KK neutrinos are shown up to $n = 4$ in the GHU model with the parameter set of $m_{\rm KK} = 13$ TeV and $\theta_H = 0.10$, and positive bulk masses of the leptons (A_+). The values of the coupling constants for neutral gauge bosons to W bosons and leptons are given in units of g_w. The values of the coupling constants for W boson to leptons are in units of $g_w/\sqrt{2}$. $g_w = e/\sin\theta_W^0$, $\sin^2\theta_W^0 = 0.2306$ (input). In the SM $\sin^2\theta_W(\overline{\rm MS}) = 0.23122 \pm 0.00004$ [12]. When the value is less than 10^{-8}, we write 0. When there is no corresponding coupling constant, we write the symbol $\cdots$ in that field.

Coupling	$n=0$	$n=1$	$n=2$	$n=3$	$n=4$
$g_{\gamma^{(n)}WW}$	$+\sin\theta_W^0$	−0.00029370	−0.00001060	−0.00000185	−0.00000052
$g_{Z^{(n)}WW}$	+0.87647017	−0.00018736	+0.00000002	−0.00000676	−0.00000002
$g_{Z_R^{(n)}WW}$	$\cdots$	+0.00027211	+0.00000980	+0.00000162	+0.00000047
$g^L_{\gamma^{(n)}ee}$	$-\sin\theta_W^0$	+0.10727367	−0.07406031	+0.06039443	−0.05245504
$g^R_{\gamma^{(n)}ee}$	$-\sin\theta_W^0$	−2.76765185	−1.08788152	−0.39449879	−0.23232603
$g^L_{Z^{(n)}ee}$	−0.30602661	+0.06795725	+0.00461504	−0.04691696	−0.00345321
$g^R_{Z^{(n)}ee}$	+0.26309454	+1.51736122	+0.00553476	+0.59638708	+0.00179601
$g^L_{Z_R^{(n)}ee}$	$\cdots$	0	0	0	0
$g^R_{Z_R^{(n)}ee}$	$\cdots$	+1.38256665	+0.55008507	+0.19760182	+0.11605766
$g^L_{We\nu_e^{(n)}}$	+0.998816639	−0.03534296	0	0	0
$g^R_{We\nu_e^{(n)}}$	0	−0.00176655	−0.01669757	−0.00000003	+0.002095116
$g^L_{We\nu_{e2}^{(n)}}$	$\cdots$	+0.03534296	0	0	0
$g^R_{We\nu_{e2}^{(n)}}$	$\cdots$	+0.00176655	−0.01669757	−0.00000003	+0.002095116

We numerically find

$$\left|\sum_a g^L_{V_aee}g_{V_aWW} + \sum_n \left(g^L_{We\nu^{(n)}}\right)^2\right| < 10^{-8}\times g_w^2,$$
$$\left|\sum_a g^R_{V_aee}g_{V_aWW} + \sum_n \left(g^R_{We\nu^{(n)}}\right)^2\right| < 10^{-8}\times g_w^2. \quad (4.46)$$

Therefore, the $O(s^2)$ and $O(s)$ terms of $\mathcal{M}^{WW}_{LL}$ and $\mathcal{M}^{WW}_{RR}$ are sufficiently suppressed. We also find that

$$\sum_n g^L_{We\nu^{(n)}}g^R_{We\nu^{(n)}}\frac{m_{\nu^{(n)}}}{m_W} \simeq 3\times 10^{-8} g_w^2. \quad (4.47)$$

The $O(s)$ term of $\mathcal{M}^{WW}_{LR}$ and $\mathcal{M}^{WW}_{RL}$ is well suppressed. Several other parameter sets are also summarized in Table VIII.

B. $e^-e^+ \to ZZ$ process

1. Amplitude

Here we consider the following t- and u-channel processes:

$$e^-_X(p_1)e^+_Y(p_2) \to Z_\mu(k_1)Z_\nu(k_2), \quad (4.48)$$

where $X, Y = L,\ R,\ \bar{L} = R,\ \bar{R} = L$; p_1 and p_2 are the momenta of the initial states of electron and positron;

TABLE VIII. The values of the coupling summation are summarized for several sets of parameters $(m_{\rm KK}, \theta_H)$ with positive bulk masses of the leptons in the units of g_w^2. When the value is less than 10^{-8}, we write 0.

$(m_{\rm KK}, \theta_H)$	SM	(13 TeV, 0.10)	(25 TeV, 0.05)	(50 TeV, 0.025)	(100 TeV, 0.0125)
$\sum_a g^L_{V_aee}g_{V_aWW}$	−0.5	−0.50006646	−0.50001791	−0.50000448	−0.50000112
$\sum_n (g^L_{We\nu^{(n)}})^2$	+0.5	+0.50006646	+0.50001791	+0.50000448	+0.50000112
$\sum_a g^R_{V_aee}g_{V_aWW}$	0	−0.00028680	−0.00006933	−0.00001731	−0.00000433
$\sum_n (g^R_{We\nu^{(n)}})^2$	0	+0.00028680	+0.00006933	+0.00001731	+0.00000433
$\sum_n g^L_{We\nu^{(n)}}g^R_{We\nu^{(n)}}\frac{m_{\nu^{(n)}}}{m_W}$	0	+0.00000003	+0.00000002	+0.00000001	0

k_1 and k_2 are the momenta of the final states of Z bosons. For massive bosons Z and massless electrons $e^{\pm}$, in the center-of-mass frame, we use the following basis:

$$\begin{aligned} p_1 &= \frac{\sqrt{s}}{2}(1,0,0,+1), \qquad p_2 = \frac{\sqrt{s}}{2}(1,0,0,-1), \\ k_1 &= \frac{\sqrt{s}}{2}(1,0,+\beta_Z \sin\theta, +\beta_Z \cos\theta), \\ k_2 &= \frac{\sqrt{s}}{2}(1,0,-\beta_Z \sin\theta, -\beta_Z \cos\theta), \end{aligned} \tag{4.49}$$

where $\beta_Z \coloneqq \sqrt{1-\frac{4m_Z^2}{s}}$. The Mandelstam variables are defined as

$$\begin{aligned} s &\coloneqq (p_1+p_2)^2 = (k_1+k_2)^2, \\ t &\coloneqq (p_1-k_1)^2 = (p_2-k_2)^2 = m_Z^2 - \frac{s}{2}(1-\beta_Z\cos\theta), \\ u &\coloneqq (p_1-k_2)^2 = (p_2-k_1)^2 = m_Z^2 - \frac{s}{2}(1+\beta_Z\cos\theta), \end{aligned} \tag{4.50}$$

where $s+t+u = 2m_Z^2$.

The contributions to the $e^-e^+ \to ZZ$ process come from t-channel and u-channel. The t-channel amplitude is given by

$$\begin{aligned} \mathcal{M}_{tXY}^{ZZ} &= \bar{v}(p_2)\gamma^\nu \left[\sum_i g_{Yi} P_Y \frac{(\not{p}_1 - \not{k}_1) + m_i}{(p_1-k_1)^2 - m_i^2}\gamma^\mu g_{Xi} P_X\right] \\ &\quad \times u(p_1)\epsilon_\mu^*(k_1)\epsilon_\nu^*(k_2) \\ &\eqqcolon K_{tXY}^{\mu\nu}\epsilon_\mu^*(k_1)\epsilon_\nu^*(k_2), \end{aligned} \tag{4.51}$$

where $P_{L/R} = (1 \mp \gamma_5)/2$, and i stands for electron and KK charged leptons. The $K_{tXY}^{\mu\nu}$ $(X,Y = L,R)$ can be written as

$$K_{tXY}^{\mu\nu} = \begin{cases} A_{tX}^{ZZ}\bar{v}(p_2)\gamma^\nu(\not{p}_1 - \not{k}_1)\gamma^\mu P_X u(p_1), & \text{for } X = Y \\ B_t^{ZZ}\bar{v}(p_2)\gamma^\nu\gamma^\mu P_X u(p_1), & \text{for } X \neq Y \end{cases}, \tag{4.52}$$

where

$$\begin{aligned} A_{tX}^{ZZ} &\coloneqq \sum_i \frac{g_{Xi}^2}{(p_1-k_1)^2 - m_i^2}, \\ B_t^{ZZ} &\coloneqq \sum_i \frac{g_{Li}g_{Ri}m_i}{(p_1-k_1)^2 - m_i^2}. \end{aligned} \tag{4.53}$$

The u-channel amplitude is given by

$$\begin{aligned} \mathcal{M}_{uXY}^{ZZ} &= \bar{v}(p_2)\gamma^\mu \left[\sum_i g_{Yi} P_Y \frac{(\not{p}_1 - \not{k}_2) + m_i}{(p_1-k_2)^2 - m_i^2}\gamma^\nu g_X P_X\right] \\ &\quad \times u(p_1)\epsilon_\mu^*(k_1)\epsilon_\nu^*(k_2) \\ &\eqqcolon K_{uXY}^{\mu\nu}\epsilon_\mu^*(k_1)\epsilon_\nu^*(k_2), \end{aligned} \tag{4.54}$$

where $P_{L/R} = (1 \mp \gamma_5)/2$. The $K_{uXY}^{\mu\nu}$ $(X,Y = L,R)$ can be written as

$$K_{uXY}^{\mu\nu} = \begin{cases} A_{uX}^{ZZ}\bar{v}(p_2)\gamma^\mu(\not{p}_1 - \not{k}_2)\gamma^\nu P_X u(p_1), & \text{for } X = Y \\ B_u^{ZZ}\bar{v}(p_2)\gamma^\mu\gamma^\nu P_X u(p_1), & \text{for } X \neq Y \end{cases}, \tag{4.55}$$

where

$$\begin{aligned} A_{uX}^{ZZ} &\coloneqq \sum_i \frac{g_{Xi}^2}{(p_1-k_2)^2 - m_i^2}, \\ B_u^{ZZ} &\coloneqq \sum_i \frac{g_{Li}g_{Ri}m_i}{(p_1-k_2)^2 - m_i^2}. \end{aligned} \tag{4.56}$$

2. Squared amplitude

The squared amplitude of the $e_X^- e_Y^+ \to ZZ$ process is given by

$$\begin{aligned} |\mathcal{M}_{XY}^{ZZ}|^2 &= |\mathcal{M}_{tXY}^{ZZ} + \mathcal{M}_{uXY}^{ZZ}|^2 \\ &= |\mathcal{M}_{tXY}^{ZZ}|^2 + |\mathcal{M}_{uXY}^{ZZ}|^2 + \mathcal{M}_{tXY}^{ZZ}\mathcal{M}_{uXY}^{ZZ\dagger} \\ &\quad + \mathcal{M}_{tXY}^{ZZ\dagger}\mathcal{M}_{uXY}^{ZZ}. \end{aligned} \tag{4.57}$$

The third and forth terms stand for the interference terms between t- and u-channel.

First, the t-channel contribution $|\mathcal{M}_{tXY}^{ZZ}|^2$ is given by

$$\begin{aligned} |\mathcal{M}_{tXY}^{ZZ}|^2 &= \sum_{\text{spins}} \epsilon_\mu^*(k_1)\epsilon_\nu^*(k_2)\epsilon_{\mu'}(k_1)\epsilon_{\nu'}(k_2) K_{tXY}^{\mu\nu}\bar{K}_{tXY}^{\mu'\nu'} \\ &= \left(-g_{\mu\mu'} + \frac{k_{1\mu}k_{1\mu'}}{k_1^2}\right)\left(-g_{\nu\nu'} + \frac{k_{2\nu}k_{2\nu'}}{k_2^2}\right) \\ &\quad \times \sum_{\text{spins}} K_{tXY}^{\mu\nu}\bar{K}_{tXY}^{\mu'\nu'}. \end{aligned} \tag{4.58}$$

Substituting Eq. (4.52) into Eq. (4.58), we find

$$|\mathcal{M}_{tXY}^{ZZ}|^2 = \begin{cases} |tA_{tX}^{ZZ}|^2\left[4\left(\frac{u}{t} - \frac{m_Z^4}{t^2}\right) + \frac{1}{m_Z^4}(ut - m_Z^4) + \frac{4s}{m_Z^2}\right] & \text{for } X = Y \\ |tB_t^{ZZ}|^2\left[\frac{4s}{t^2} + \frac{s}{m_Z^4} + \frac{4}{m_Z^2}\left(\frac{u}{t} - \frac{m_Z^4}{t^2}\right)\right] & \text{for } X \neq Y \end{cases}. \tag{4.59}$$

Next, the u-channel contribution $|\mathcal{M}^{ZZ}_{uXY}|^2$ is given by

$$|\mathcal{M}^{ZZ}_{u}|^2 = \sum_{\text{spins}} \epsilon^*_\mu(k_1)\epsilon^*_\nu(k_2)\epsilon_{\mu'}(k_1)\epsilon_{\nu'}(k_2) K^{\mu\nu}_u \bar{K}^{\mu'\nu'}_u$$
$$= \left(-g_{\mu\mu'} + \frac{k_{1\mu}k_{1\mu'}}{k_1^2}\right)\left(-g_{\nu\nu'} + \frac{k_{2\nu}k_{2\nu'}}{k_2^2}\right)\sum_{\text{spins}} K^{\mu\nu}_u \bar{K}^{\mu'\nu'}_u . \tag{4.60}$$

Substituting Eq. (4.55) into Eq. (4.60), we find

$$|\mathcal{M}^{ZZ}_{uXY}|^2 = \begin{cases} |uA^{ZZ}_{uX}|^2\left[4\left(\frac{t}{u} - \frac{m_Z^4}{u^2}\right) + \frac{1}{m_Z^4}\left(ut - m_Z^4\right) + \frac{4s}{m_Z^2}\right] & \text{for } X = Y \\ |uB^{ZZ}_{u}|^2\left[\frac{4s}{u^2} + \frac{s}{m_Z^4} + \frac{4}{m_Z^2}\left(\frac{t}{u} - \frac{m_Z^4}{u^2}\right)\right] & \text{for } X \neq Y \end{cases}. \tag{4.61}$$

Finally, the interference terms are given by

$$\mathcal{M}^{ZZ}_{t}\mathcal{M}^{ZZ\dagger}_{u} + \mathcal{M}^{ZZ\dagger}_{t}\mathcal{M}^{ZZ}_{u} = \sum_{\text{spins}} \epsilon^*_\mu(k_1)\epsilon^*_\nu(k_2)\epsilon_{\mu'}(k_1)\epsilon_{\nu'}(k_2)\left(K^{\mu\nu}_t \bar{K}^{\mu'\nu'}_u + \bar{K}^{\mu\nu}_t K^{\mu'\nu'}_u\right)$$
$$= \left(-g_{\mu\mu'} + \frac{k_{1\mu}k_{1\mu'}}{k_1^2}\right)\left(-g_{\nu\nu'} + \frac{k_{2\nu}k_{2\nu'}}{k_2^2}\right)\sum_{\text{spins}}\left(K^{\mu\nu}_t \bar{K}^{\mu'\nu'}_u + \bar{K}^{\mu\nu}_t K^{\mu'\nu'}_u\right) \tag{4.62}$$

Substituting Eqs. (4.52) and (4.55) into Eq. (4.62), we find

$$\mathcal{M}^{ZZ}_{tXY}\mathcal{M}^{ZZ\dagger}_{uXY} + \mathcal{M}^{ZZ\dagger}_{tXY}\mathcal{M}^{ZZ}_{uXY} = \begin{cases} ut(A^{ZZ}_{tX}A^{ZZ*}_{uX} + A^{ZZ}_{uX}A^{ZZ*}_{tX}) \cdot \left\{\frac{8m_Z^2 s}{ut} + \frac{m_Z^4 - ut}{m_Z^4} - \frac{4s}{m_Z^2}\right\} & \text{for } X = Y \\ ut(B^{ZZ}_{t}B^{ZZ*}_{u} + B^{ZZ}_{u}B^{ZZ*}_{t}) \cdot \left\{\frac{8s}{ut} + \frac{2s}{m_Z^4} - \frac{4(m_Z^2-u)(m_Z^2-t)}{ut}\right\} & \text{for } X \neq Y \end{cases}. \tag{4.63}$$

From Eqs. (4.59), (4.61), and (4.63), the total amplitudes of $e^-_X e^+_Y \to ZZ$ are given by for $X = Y$

$$|\mathcal{M}^{ZZ}_{XY}|^2 = |tA^{ZZ}_{tX}|^2\left\{4\left(\frac{u}{t} - \frac{m_Z^4}{t^2}\right) + \frac{1}{m_Z^4}(ut - m_Z^4) + \frac{4s}{m_Z^2}\right\}$$
$$+ |uA^{ZZ}_{uX}|^2\left\{4\left(\frac{t}{u} - \frac{m_Z^4}{u^2}\right) + \frac{1}{m_Z^4}(ut - m_Z^4) + \frac{4s}{m_Z^2}\right\}$$
$$+ 2\text{Re}[tA^{ZZ}_{tX} \cdot uA^{ZZ*}_{uX}]\left\{\frac{8m_Z^2 s}{ut} + \frac{m_Z^4 - ut}{m_Z^4} - \frac{4s}{m_Z^2}\right\}; \tag{4.64}$$

and for $X \neq Y$

$$2|\mathcal{M}^{ZZ}_{XY}|^2 = |tB^{ZZ}_{t}|^2\left\{\frac{8s}{t^2} + \frac{2s}{m_Z^4} + \frac{8}{m_Z^2}\left(\frac{u}{t} - \frac{m_Z^4}{t^2}\right)\right\}$$
$$+ |uB^{ZZ}_{u}|^2\left\{\frac{8s}{u^2} + \frac{2s}{m_Z^4} + \frac{8}{m_Z^2}\left(\frac{t}{u} - \frac{m_Z^4}{u^2}\right)\right\}$$
$$+ \left(2\text{Re}[tB^{ZZ}_{t}uB^{ZZ*}_{u}]\right)$$
$$\cdot \left\{\frac{8s}{ut} + \frac{2s}{m_Z^4} - \frac{4(m_Z^2 - t)(m_Z^2 - u)}{ut}\right\}. \tag{4.65}$$

3. Cross section

For the $e^-_X e^+_Y \to ZZ$ process, the cross section of the initial states of the polarized electron and positron is given by

$$\frac{d\sigma^{ZZ}}{d\cos\theta}(P_{e^-}, P_{e^+}, \cos\theta) = \frac{1}{4}\left\{(1 - P_{e^-})(1 + P_{e^+})\frac{d\sigma^{ZZ}_{LL}}{d\cos\theta}\right.$$
$$+ (1 + P_{e^-})(1 - P_{e^+})\frac{d\sigma^{ZZ}_{RR}}{d\cos\theta}$$
$$+ (1 - P_{e^-})(1 - P_{e^+})\frac{d\sigma^{ZZ}_{LR}}{d\cos\theta}$$
$$\left. + (1 + P_{e^-})(1 + P_{e^+})\frac{d\sigma^{ZZ}_{RL}}{d\cos\theta}\right\}, \tag{4.66}$$

where P_{e^-} and P_{e^+} are the initial polarizations of the electron and positron

$$\frac{d\sigma^{ZZ}_{XY}}{d\cos\theta}(\cos\theta) \coloneqq \frac{d\sigma}{d\cos\theta}\left(e^-_X e^+_Y \to ZZ\right) = \frac{\beta_Z}{32\pi s}|\mathcal{M}^{ZZ}_{XY}|^2, \tag{4.67}$$

where $\mathcal{M}^{ZZ}_{XY}$ are given in Eqs. (4.64) and (4.65)

The total cross section of the $e^-e^+ \to ZZ$ process with the initial polarizations can be defined by integrating the differential cross section in Eq. (4.66) with the angle θ

$$\sigma^{ZZ}(P_{e^-}, P_{e^+}) \coloneqq \frac{1}{2}\int_{-1}^{1} \frac{d\sigma^{ZZ}}{d\cos\theta}(P_{e^-}, P_{e^+}, \cos\theta) d\cos\theta, \tag{4.68}$$

where the minimum and maximal values of $\cos\theta$ are determined by each detector and we cannot use date near $\cos\theta \simeq \pm 1$. The total cross section of $e^-e^+ \to ZZ$ is given by

$$\begin{aligned}\sigma^{ZZ}(P_{e^-}, P_{e^+}) = &\frac{1}{4}(1-P_{e^-})(1+P_{e^+})\sigma^{ZZ}_{LL} \\ &+\frac{1}{4}(1+P_{e^-})(1-P_{e^+})\sigma^{ZZ}_{RR} \\ &+\frac{1}{4}(1-P_{e^-})(1-P_{e^+})\sigma^{ZZ}_{LR} \\ &+\frac{1}{4}(1+P_{e^-})(1+P_{e^+})\sigma^{ZZ}_{RL},\end{aligned} \tag{4.69}$$

where

$$\sigma^{ZZ}_{XY} \coloneqq \frac{1}{2}\int_{-1}^{1} \frac{d\sigma^{ZZ}_{XY}}{d\cos\theta}(\cos\theta) d\cos\theta, \tag{4.70}$$

where $X = L, R$; $d\sigma^{ZZ}_{XY}/d\cos\theta$ are given in Eq. (4.67).

The statistical error of the cross section $\sigma^{ZZ}(P_{e^-}, P_{e^+})$ is given by

$$\begin{aligned}\Delta\sigma^{ZZ}(P_{e^-}, P_{e^+}) &= \frac{\sigma^{ZZ}(P_{e^-}, P_{e^+})}{\sqrt{N^{ZZ}}}, \\ N^{ZZ} &= L_{\rm int} \cdot \sigma^{ZZ}(P_{e^-}, P_{e^+}),\end{aligned} \tag{4.71}$$

where $L_{\rm int}$ is an integrated luminosity, and N^{ZZ} is the number of events for the $e^-e^+ \to ZZ$ process. Note that the Z boson cannot be observed directly, so we need to choose the decay modes of the Z boson, and then the available number of events must be N^{ZZ} multiplied by the branching ratio of each selected decay mode. The amount of the deviation of the cross section of the $e^-e^+ \to ZZ$ process from the SM in the GHU model is given by

$$\Delta^{ZZ}_{\sigma}(P_{e^-}, P_{e^+}) \coloneqq \frac{[\sigma^{ZZ}(P_{e^-}, P_{e^+})]_{\rm GHU}}{[\sigma^{ZZ}(P_{e^-}, P_{e^+})]_{\rm SM}} - 1, \tag{4.72}$$

where $[\sigma^{ZZ}(P_{e^-}, P_{e^+})]_{\rm GHU}$ and $[\sigma^{ZZ}(P_{e^-}, P_{e^+})]_{\rm SM}$ stand for the cross sections of the $e^-e^+ \to ZZ$ process in the SM and the GHU model, respectively. The same notation is used for other cases in the followings.

4. Left-right asymmetry

We define an observable left-right asymmetry of the $e^-e^+ \to ZZ$ process as

$$A^{ZZ}_{LR}(P_{e^-}, P_{e^+}) \coloneqq \frac{\sigma^{ZZ}(P_{e^-}, P_{e^+}) - \sigma^{ZZ}(-P_{e^-}, -P_{e^+})}{\sigma^{ZZ}(P_{e^-}, P_{e^+}) + \sigma^{ZZ}(-P_{e^-}, -P_{e^+})} \tag{4.73}$$

for $P_{e^-} < 0$ and $|P_{e^-}| > |P_{e^+}|$.

The statistical error of the left-right asymmetry is given by

$$\Delta A^{ZZ}_{LR}(P_{e^-}, P_{e^+}) = 2\frac{\sqrt{N^{ZZ}_L N^{ZZ}_R}\left(\sqrt{N^{ZZ}_L} + \sqrt{N^{ZZ}_R}\right)}{\left(N^{ZZ}_L + N^{ZZ}_R\right)^2}, \tag{4.74}$$

where $N^{ZZ}_L = L_{\rm int}\sigma^{ZZ}(P_{e^-}, P_{e^+})$ and $N^{ZZ}_R = L_{\rm int}\sigma^{ZZ}(-P_{e^-}, -P_{e^+})$ are the numbers of the events for $P_{e^-} < 0$ and $|P_{e^-}| > |P_{e^+}|$. The amount of the deviation from the SM in Eq. (4.73) is characterized by

$$\Delta^{ZZ}_{A_{LR}}(P_{e^-}, P_{e^+}) \coloneqq \frac{[A^{ZZ}_{LR}(P_{e^-}, P_{e^+})]_{\rm GHU}}{[A^{ZZ}_{LR}(P_{e^-}, P_{e^+})]_{\rm SM}} - 1. \tag{4.75}$$

V. NUMERICAL ANALYSIS

We analyze cross sections of W and Z boson pair production processes $e^-e^+ \to W^-W^+$ and $e^-e^+ \to ZZ$ for the initial states of unpolarized and polarized electrons and positrons, where we use the formula of the cross sections given in Sec. IV. For the values of the initial polarizations, we mainly use $(P_{e^-}, P_{e^+}) = (\mp 0.8, \pm 0.3)$ with the ILC experiment in mind.

A. $e^-e^+ \to W^-W^+$

Here we evaluate observables of the $e^-e^+ \to W^-W^+$ process in the SM and the GHU model at tree level. We use the parameter sets $\mathrm{A}_\pm$, $\mathrm{B}_\pm$, $\mathrm{C}_\pm$ listed in Tables I, II, and IV.

In Fig. 2, we show the total cross sections of the $e^-e^+ \to W^-W^+$ process in the SM and the GHU model in wider range of $\sqrt{s}$ with unpolarized and polarized electron and positron beams, where $A_\pm$, $B_\pm$, $C_\pm$ are the names of the parameter sets listed in Table I. From Fig. 2, we can see that the deviation from the SM of the GHU model is very large due to the effect of resonances around the mass scale of the Z' bosons. We focus on the cross sections around $\sqrt{s} \simeq 10$ TeV for $A_\pm$. Three Z' bosons $\gamma^{(1)}$, $Z^{(1)}$, and $Z^{(1)}_R$ contribute to this resonance via the s-channel process, where this system take place very strong cancellation between s-channel, t-channel, and interference terms. The mass of $Z^{(1)}_R$ is slightly smaller than the masses of $\gamma^{(1)}$ and $Z^{(1)}$ and the sign of the coupling constants to the electrons and W bosons varies with the sign of the bulk mass parameters given in Tables II, IV, and VIII in Ref. [57], For $A_p m$, the coupling constants of the Z' bosons to

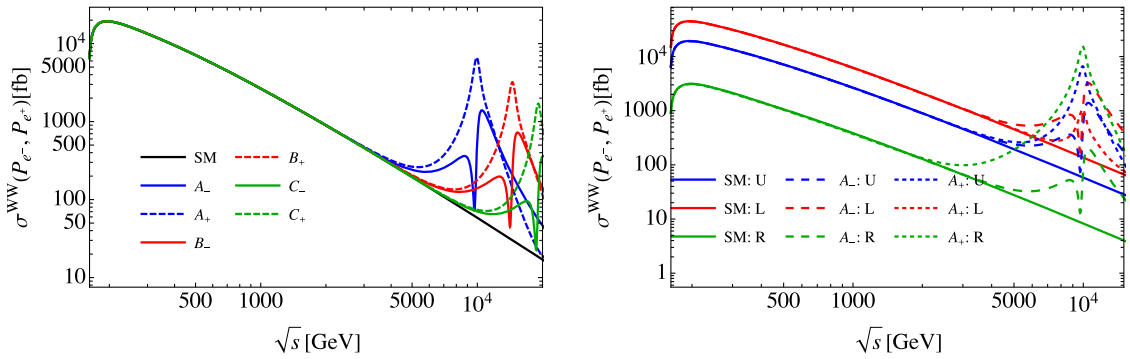

FIG. 2. The total cross sections of the $e^-e^+ \to W^-W^+$ process in the SM and the GHU model are shown in wider range of $\sqrt{s}$. The left figure shows the $\sqrt{s}$ dependence of $\sigma^{WW}(P_{e^-} = 0, P_{e^+} = 0)$ in the SM and the GHU model with unpolarized electron and positron beams, where $A_\pm$, $B_\pm$, $C_\pm$ are the names of the parameter sets listed in Table I. The right figure shows the $\sqrt{s}$ dependence of $\sigma^{WW}(P_{e^-}, P_{e^+})$ in the SM and the GHU model whose parameter set is A_- with the three different polarizations U, L, R, where U, L, R stand for $(P_{e^-}, P_{e^+}) = (0, 0), (-0.8, +0.3), (+0.8, -0.3)$, respectively.

electrons and W bosons are given in Tables V and VII. In the A_- case, the combination is caused by interference effects among the SM gauge bosons and Z' bosons at energies slightly below the mass of $Z_R^{(1)}$. In the case of A_+, on the other hand, the sign of the coupling constants is such that no interference occurs.

In Fig. 3, we show the angular distribution of the cross sections of the $e^-e^+ \to W^-W^+$ process in the SM with $(P_{e^-}, P_{e^+}) = (0, 0)$ at $\sqrt{s} = 250$ GeV and 500 GeV with unpolarized $e^\pm$ beams, where $\sigma^{WW}(P_{e^-}, P_{e^+})$ given in Eq. (4.23). Figure 3 shows that except for $\cos\theta \simeq 1$, there is very strong cancellation among the s-channel, t-channel, and interference terms. Furthermore, the larger $\sqrt{s}$, the more the forward cross section increases while the backward cross section cancels out more strongly.

In Fig. 4, the deviations from the SM in the GHU with polarized $e^\pm$ beams are shown. The deviation from the SM in the GHU model with unpolarized and left- and right-handed polarized $e^\pm$ beams $(P_{e^-}, P_{e^+}) = (0, 0)$, $(-0.8, +0.3), (+0.8, -0.3)$, respectively. The statistical errors in the SM are estimated by using leptonic decays $W^\pm \to \ell^\pm\nu$. Since $\mathrm{Br}(W^+ \to \ell^+\nu) = (10.86 \pm 0.09)\%$ [12], the branching ratio of $W^+W^- \to \ell^-\ell'^+\nu\nu'$ is 10.615%. The estimates from the statistical errors in this figure show that the exploration area for the GHU model is wider for $\sqrt{s} = 500$ GeV, $L_{\mathrm{int}} = 1\mathrm{ab}^{-1}$ than for $\sqrt{s} = 250$ GeV, $L_{\mathrm{int}} = 2\mathrm{ab}^{-1}$. We also find that for the A_-, B_-, C_- cases, where the bulk masses are negative, the deviation from the SM is larger in the left-handed $e^\pm$ beams because the left-handed coupling constants are larger than the right-handed ones, while for the A_+, B_+, C_+ cases, where the bulk masses are positive, the deviation from the SM is larger in the right-handed $e^\pm$ beams because the right-handed coupling constants are larger than the left-handed ones.

From Fig. 5, the total cross sections of the $e^-e^+ \to W^-W^+$ process in the SM and the GHU model are shown in range of $\sqrt{s} = [165, 1000]$ GeV. The left figure shows the $\sqrt{s}$ dependence of $\sigma^{WW}(P_{e^-} = 0, P_{e^+} = 0)$ in the SM with unpolarized electron and positron beams, Total stands for differential cross section including all the contribution from

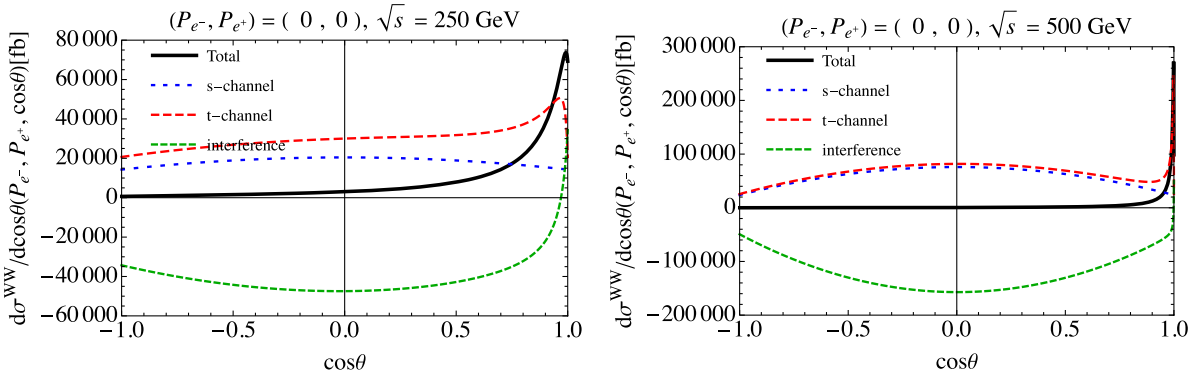

FIG. 3. The differential cross sections of the $e^-e^+ \to W^-W^+$ process in the SM $\frac{d\sigma^{WW}}{d\cos\theta}(P_{e^-}, P_{e^+}, \cos\theta)$ are shown at $\sqrt{s} = 250$ GeV and 500 GeV for the left and right figures, respectively. Total stands for differential cross section including all the contribution from s-channel, t-channel, and interference terms. s-channel, t-channel, and interference stand for differential cross section only including each contribution.

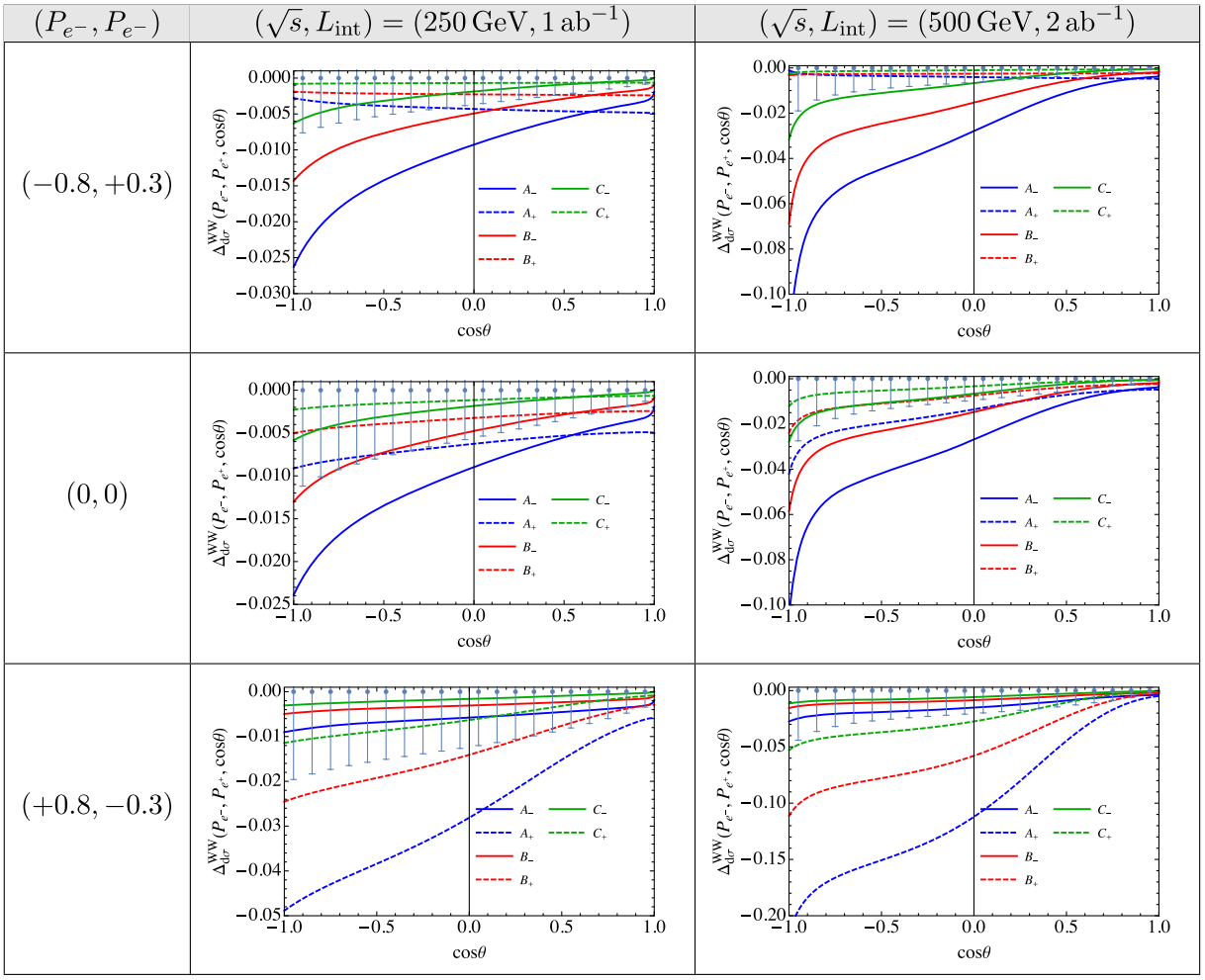

FIG. 4. The deviations from the SM in the GHU for the $e^-e^+ \to W^-W^+$ process $\Delta^{WW}_{d\sigma}(P_{e^-}, P_{e^+}, \cos\theta)$ are shown with $(P_{e^-}, P_{e^+}) = (-0.8, +0.3), (0, 0), (+0.8, -0.3)$ for upper, middle and lower rows, respectively, where $\Delta^{WW}_{d\sigma}(P_{e^-}, P_{e^+}, \cos\theta) \coloneqq [\frac{d\sigma^{WW}}{d\cos\theta}(P_{e^-}, P_{e^+}, \cos\theta)]_{\rm GHU}[\frac{d\sigma^{WW}}{d\cos\theta}(P_{e^-}, P_{e^+}, \cos\theta)]^{-1}_{\rm SM} - 1$. The left and right side figures show the deviation at $\sqrt{s} = 250$ GeV and 500 GeV, respectively. The error bars represent statistical errors in the SM at $\sqrt{s} = 250$ GeV with 1 ab^{-1} data and at $\sqrt{s} = 500$ GeV with 2 ab^{-1} data by using leptonic decays $W^\pm \to \ell^\pm\nu$. The branching ratio of $W^+W^- \to \ell^-\ell'^+\nu\nu'$ is 10.615% since ${\rm Br}(W^+ \to \ell^+\nu) = (10.86 \pm 0.09)\%$ [12]. Each bin is given by $\cos\theta = [k - 0.05, k + 0.05]$ $(k = -0.95, -0.85, \ldots, 0.95)$.

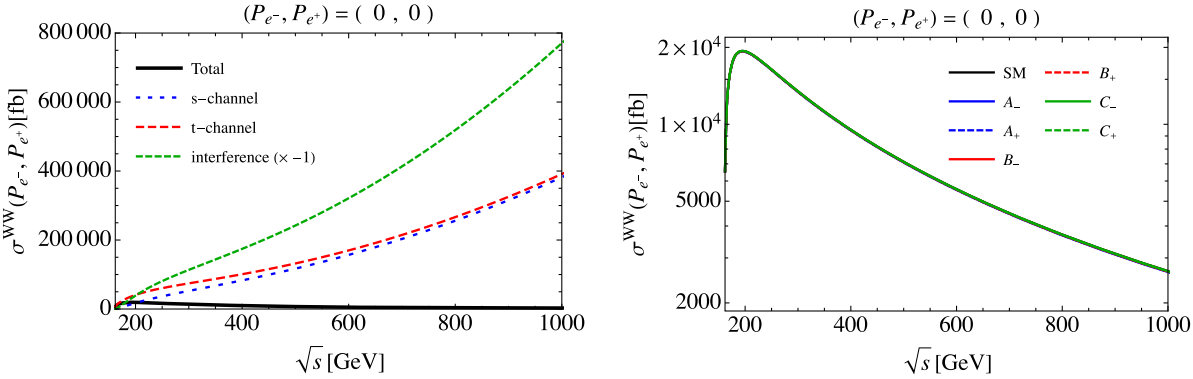

FIG. 5. The total cross sections of the $e^-e^+ \to W^-W^+$ process in the SM and the GHU model $\sigma^{WW}(P_{e^-}, P_{e^+})$ are shown in range of $\sqrt{s} = [165, 1000]$ GeV. The left figure shows the $\sqrt{s}$ dependence of $\sigma^{WW}(P_{e^-} = 0, P_{e^+} = 0)$ in the SM with unpolarized electron and positron beams, Total stands for differential cross section including all the contribution from s-channel, t-channel, and interference terms. s-channel, t-channel, and interference stand for cross section only including each contribution. The right figure shows the $\sqrt{s}$ dependence of $\sigma^{WW}(P_{e^-}, P_{e^+})$ in the SM and the GHU model whose parameters set are $A_\pm$, $B_\pm$, $C_\pm$.

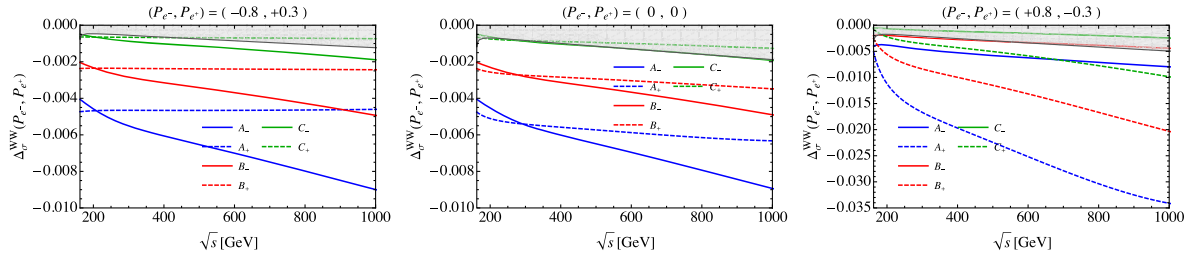

FIG. 6. The $\sqrt{s}$ dependence of the deviation from the SM in the GHU models for the total cross sections, $\Delta_\sigma^{WW}(P_{e^-}, P_{e^+})$, is shown for $(P_{e^-}, P_{e^+}) = (-0.8, +0.3), (0, 0), (+0.8, -0.3)$, respectively, where $\Delta_\sigma^{WW}(P_{e^-}, P_{e^+}) \coloneqq [\sigma^{WW}(P_{e^-}, P_{e^+})]_{\rm GHU}/[\sigma^{WW}(P_{e^-}, P_{e^+})]_{\rm SM} - 1$. The gray region represents the 1σ statistical error estimated by using leptonic decays $W^\pm \to \ell^\pm \nu$ and the integrated luminosity $L_{\rm int} = 1\ {\rm ab}^{-1}$.

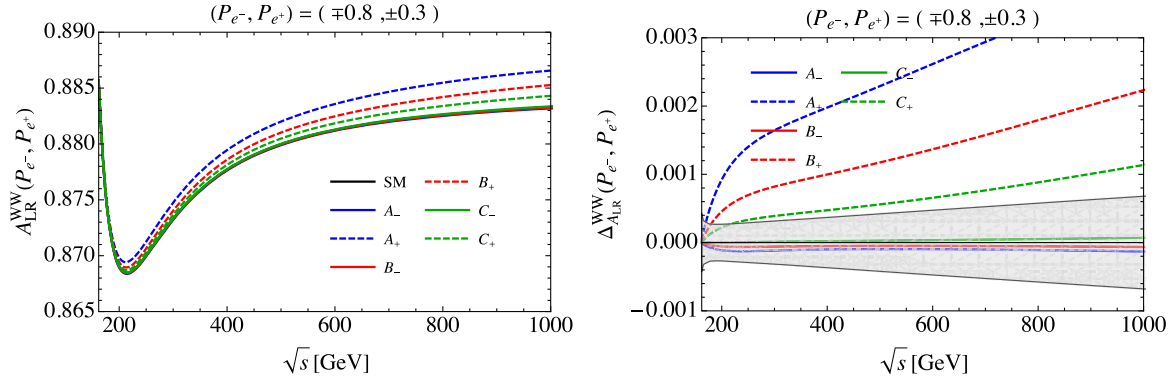

FIG. 7. The $\sqrt{s}$ dependence of the left-right asymmetry of the $e^-e^+ \to W^-W^+$ process and the deviation from the SM are shown. The left figure shows the $\sqrt{s}$ dependence of $A_{LR}^{WW}(P_{e^-}, P_{e^+})$ in the SM and the GHU model. The right figure shows the $\sqrt{s}$ dependence of $\Delta_{A_{LR}}^{WW}(P_{e^-}, P_{e^+})$, where $\Delta_{A_{LR}}^{WW}(P_{e^-}, P_{e^+}) \coloneqq [A_{LR}^{WW}(P_{e^-}, P_{e^+})]_{\rm GHU}/[A_{LR}^{WW}(P_{e^-}, P_{e^+})]_{\rm SM} - 1$. The energy ranges $\sqrt{s}$ in the first and second figures are $\sqrt{s} = [200, 3000]$ GeV, $\sqrt{s} = [200, 1000]$ GeV, respectively. The gray region represents the 1σ statistical error in the SM at each $\sqrt{s}$ with 1 ab^{-1} for each polarized initial states $(P_{e^-}, P_{e^+}) = (\mp 0.8, \pm 0.3)$ by using the total cross section of W boson pair production.

s-channel, t-channel, and interference terms. s-channel, t-channel, and interference stand for cross section only including each contribution. The right figure shows the $\sqrt{s}$ dependence of $\sigma^{WW}(P_{e^-}, P_{e^+})$ in the SM and the GHU model whose parameters set are $A_\pm$, $B_\pm$, $C_\pm$. From the left figure, we can see that for larger $\sqrt{s}$, stronger cancellation between s-channel, t-channel, and interference terms is taking place. This figure shows the SM case, but the same phenomenon occurs in the GHU model. From the right figure, we find that the cross sections in the GHU with the parameter sets $A_\pm$, $B_\pm$, $C_\pm$ are almost the same as that in the SM.

In Fig. 6, the $\sqrt{s}$ dependence of the deviation from the SM in the GHU models for the total cross sections, $\Delta_\sigma^{WW}(P_{e^-}, P_{e^+})$, is shown, where $\Delta_\sigma^{WW}(P_{e^-}, P_{e^+})$ is given in Eq. (4.29). The 1σ statistical errors are estimated by using the total cross section of W boson pair production. We find that for the A_-, B_-, C_- cases, where the bulk masses are negative, the deviation from the SM is larger in the left-handed $e^\pm$ beams, while for the A_+, B_+, C_+ cases, where the bulk masses are positive, the deviation from the SM is larger in the right-handed $e^\pm$ beams.

In Fig. 7, the $\sqrt{s}$ dependence of the left-right asymmetry A_{LR}^{WW} of the $e^-e^+ \to W^-W^+$ processes and the deviation from the SM $\Delta_{A_{LR}}^{WW}$ are shown, where A_{LR}^{WW} and $\Delta_{A_{LR}}^{WW}$ are given in Eqs. (4.30) and (4.32), respectively. The 1σ statistical error in the SM at each $\sqrt{s}$ with 1 ab^{-1} for each polarized initial electron and positron $(P_{e^-}, P_{e^+}) = (\mp 0.8, \pm 0.3)$ is estimated by using the total cross section of W boson pair production and the branching ratio of $W^\pm \to \ell^\pm \nu$. From Fig. 7, we find that by using the left-right asymmetry A_{LR}^{WW} we can explore higher KK scales than the constraints from the LHC experiment only for the positive bulk mass.

B. $e^-e^+ \to ZZ$

Here we evaluate observables of the $e^-e^+ \to ZZ$ process in the SM and the GHU model at tree level. As the same in Sec. V A, we use the parameter sets $A_\pm$, $B_\pm$, $C_\pm$ listed in Tables I, II, and IV.

In Fig. 8, we show the total cross sections of the $e^-e^+ \to ZZ$ process in the SM and the GHU model in wider range

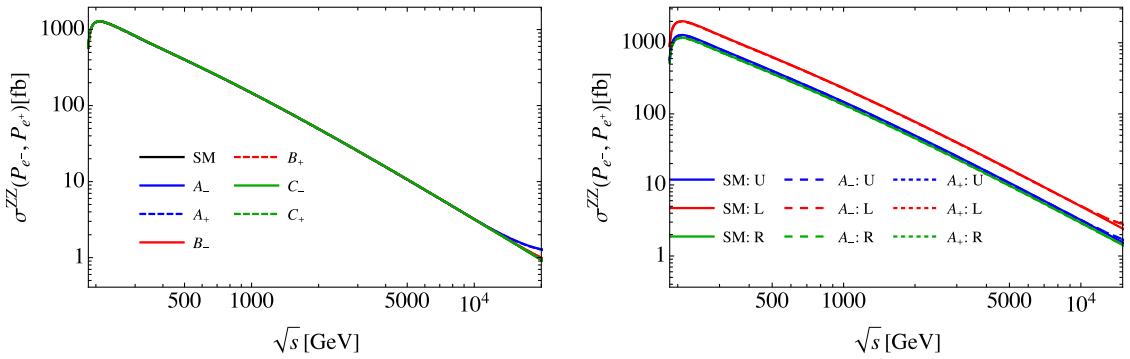

FIG. 8. The total cross sections of the $e^-e^+ \to ZZ$ process in the SM and the GHU model $\sigma^{ZZ}(P_{e^-}, P_{e^+})$ are shown in wider range of $\sqrt{s}$. The left figure shows the $\sqrt{s}$ dependence of $\sigma^{ZZ}(P_{e^-} = 0, P_{e^+} = 0)$ in the SM and the GHU model with unpolarized electron and positron beams, where $A_\pm$, $B_\pm$, $C_\pm$ are the names of the parameter sets listed in Table I. The right figure shows the $\sqrt{s}$ dependence of $\sigma^{ZZ}(P_{e^-}, P_{e^+})$ in the SM and the GHU model whose parameter sets are $A_\pm$ with the three different polarizations U, L, R, where U, L, R stand for $(P_{e^-}, P_{e^+}) = (0, 0), (-0.8, +0.3), (+0.8, -0.3)$, respectively.

of $\sqrt{s}$ with unpolarized and polarized electron and positron beams. Unlike the $e^-e^+ \to W^-W^+$ process, the $e^-e^+ \to ZZ$ process has only t- and u-channel contributions, so there are no resonances even near the Z' bosons.

In Fig. 9, we show the angular distribution of the differential cross sections of the $e^-e^+ \to W^-W^+$ process at $\sqrt{s} = 250$ GeV and 500 GeV with unpolarized $e^\pm$ beams $(P_{e^-}, P_{e^+}) = (0, 0)$. Figure 9 shows that except for $\cos\theta \simeq \pm 1$, there is very strong cancellation among the t-channel, u-channel, and interference terms. Furthermore, the larger $\sqrt{s}$, the more the forward and backward cross sections increase.

In Fig. 10, the deviations from the SM in the GHU with polarized $e^\pm$ beams are shown. The deviation from the SM in the GHU model with unpolarized and left- and right-handed polarized $e^\pm$ beams $(P_{e^-}, P_{e^+}) = (0, 0), (-0.8, +0.3), (+0.8, -0.3)$. Figure 10 shows that the deviation from the SM is small for all the parameter sets. The statistical errors in the SM are estimated by using leptonic decays $Z \to \ell^+\ell^-$. Since $\mathrm{Br}(Z \to \ell^+\ell^-) = (3.3658 \pm 0.0023)\%$ [12], the branching ratio of $ZZ \to \ell^-\ell^+\ell'^-\ell'^+$ is 1.019%. It can be seen that while the decay to charged leptons can be measured precisely, the statistical errors are overwhelmingly insufficient to see the deviation from the SM in the GHU model. It may be possible to see the deviation of the GHU model from the SM by using the decay modes of the Z bosons to hadrons, where the branching ratio of the Z bosons to hadrons is about 70% and the branching ratio of the Z bosons to leptons and hadrons is about 10%. Therefore, it may be possible to explore up to the KK mass scale beyond current experimental limits if the systematic errors in the decay of Z bosons into hadrons can be sufficiently suppressed.

From Fig. 11, the total cross sections of the $e^-e^+ \to ZZ$ process in the SM and the GHU model are shown in range of $\sqrt{s} = [185, 1000]$ GeV. The left figure shows the $\sqrt{s}$ dependence of $\sigma^{WW}(P_{e^-} = 0, P_{e^+} = 0)$ in the SM with unpolarized electron and positron beams, Total stands for

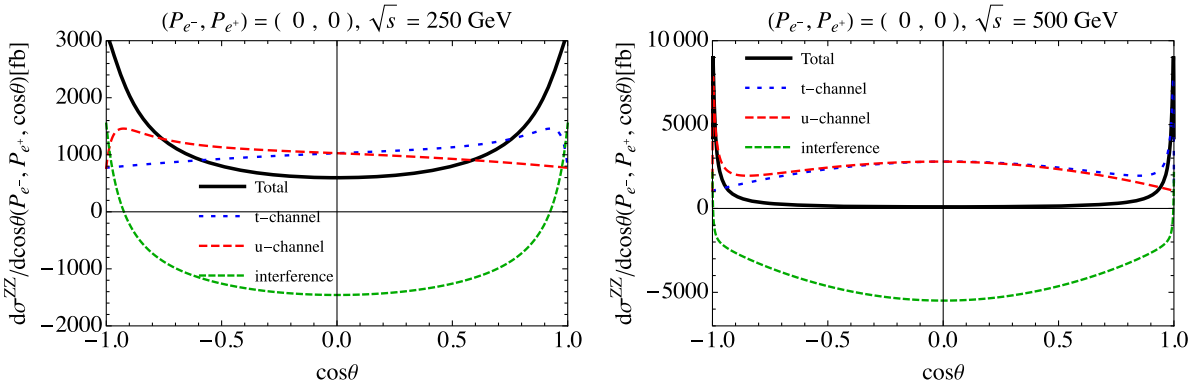

FIG. 9. The differential cross sections of the $e^-e^+ \to ZZ$ process in the SM with unpolarized electron and positron beams $\frac{d\sigma^{ZZ}}{d\cos\theta}(P_{e^-}, P_{e^+}, \cos\theta)$ are shown at $\sqrt{s} = 250$ GeV and 500 GeV for the left and right figures, respectively. Total stands for differential cross section including all the contribution from s-channel, t-channel, and interference terms. s-channel, t-channel, and interference stand for cross section only including each contribution.

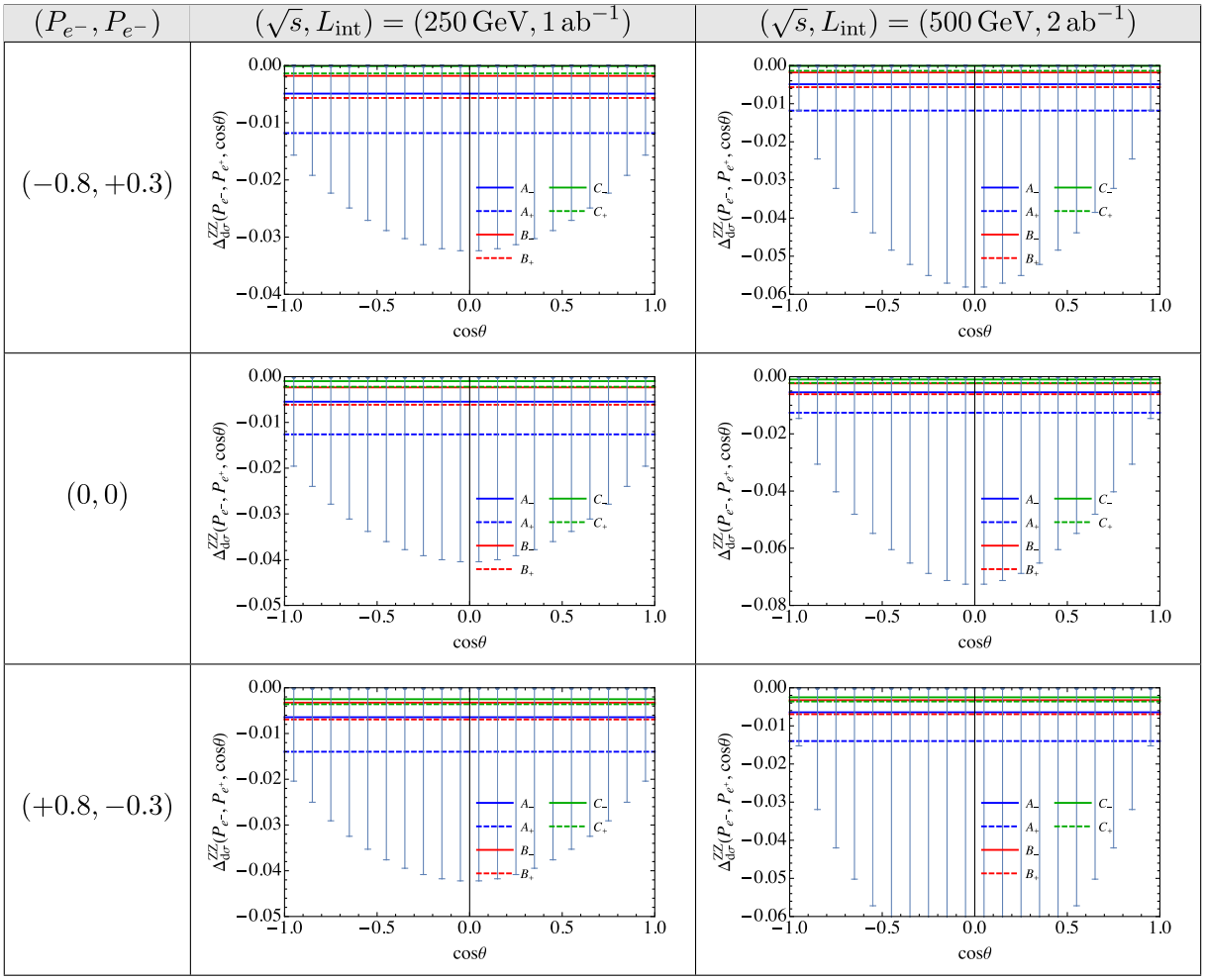

FIG. 10. The deviations from the SM in the GHU for the $e^-e^+ \to ZZ$ process $\Delta^{ZZ}_{d\sigma}(P_{e^-}, P_{e^+}, \cos\theta)$ are shown with $(P_{e^-}, P_{e^+}) = (-0.8, +0.3), (0, 0), (+0.8, -0.3)$ for upper, middle and lower rows, respectively, where $\Delta^{ZZ}_{d\sigma}(P_{e^-}, P_{e^+}, \cos\theta) \coloneqq [\frac{d\sigma^{ZZ}}{d\cos\theta}(P_{e^-}, P_{e^+})]_{\rm GHU}[\frac{d\sigma^{ZZ}}{d\cos\theta}(P_{e^-}, P_{e^+})]^{-1}_{\rm SM} - 1$. The left and right side figures show the deviation at $\sqrt{s} = 250$ GeV and 500 GeV, respectively. The error bars represent statistical errors in the SM at $\sqrt{s} = 250$ GeV with 1 ab^{-1} data and at $\sqrt{s} = 500$ GeV with 2 ab^{-1} data by using leptonic decays $Z \to \ell^+\ell^-$. Each bin is given by $\cos\theta = [k - 0.05, k + 0.05]$ $(k = -0.95, -0.85, \ldots, 0.95)$. Note that ${\rm Br}(Z \to \ell^+\ell^-) = (3.3658 \pm 0.0023)\%$ [12].

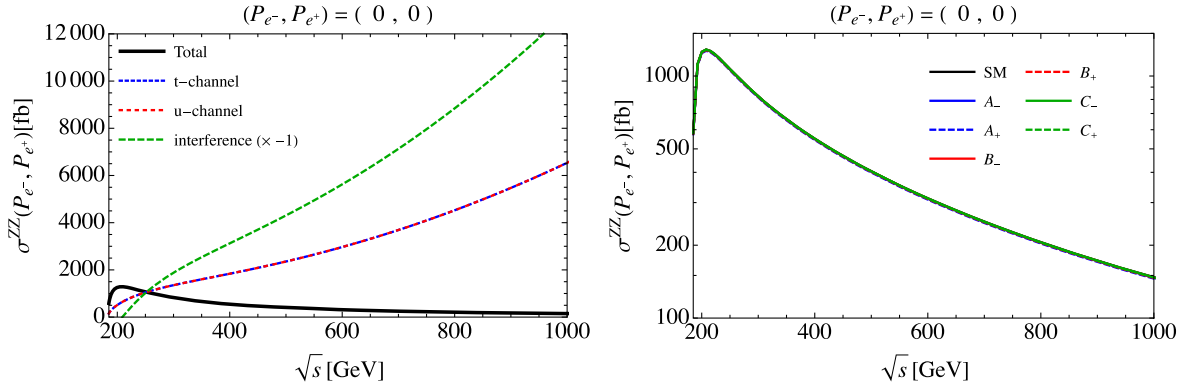

FIG. 11. The total cross sections of the $e^-e^+ \to ZZ$ process in the SM and the GHU model $\sigma^{ZZ}(P_{e^-}, P_{e^+})$ are shown in range of $\sqrt{s} = [185, 1000]$ GeV. The left figure shows the $\sqrt{s}$ dependence of $\sigma^{ZZ}(P_{e^-} = 0, P_{e^+} = 0)$ in the SM with unpolarized electron and positron beams, Total stands for differential cross section including all the contribution from s-channel, t-channel, and interference terms. s-channel, t-channel, and interference stand for cross section only including each contribution. The right figure shows the $\sqrt{s}$ dependence of $\sigma^{ZZ}(P_{e^-}, P_{e^+})$ in the SM and the GHU model whose parameters set are $A_\pm$, $B_\pm$, $C_\pm$.

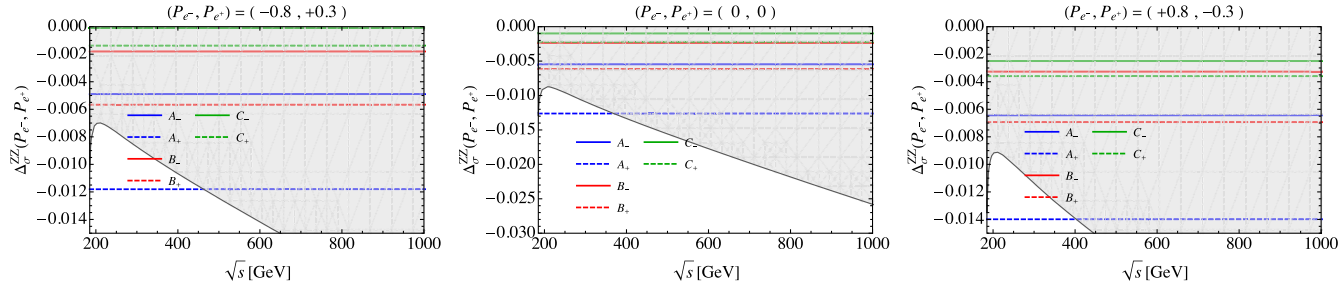

FIG. 12. The $\sqrt{s}$ dependence of the deviation from the SM in the GHU models for the total cross sections, $\Delta_\sigma^{ZZ}(P_{e^-}, P_{e^+})$, is shown for $(P_{e^-}, P_{e^+}) = (-0.8, +0.3), (0, 0), (+0.8, -0.3)$, respectively, where $\Delta_\sigma^{ZZ}(P_{e^-}, P_{e^+}) \coloneqq [\sigma^{ZZ}(P_{e^-}, P_{e^+})]_{\mathrm{GHU}}/[\sigma^{ZZ}(P_{e^-}, P_{e^+})]_{\mathrm{SM}} - 1$. The gray region represents the 1σ statistical error estimated by using the total cross section of Z boson pair production and integrated luminosity $L_{\mathrm{int}} = 1\ \mathrm{ab}^{-1}$.

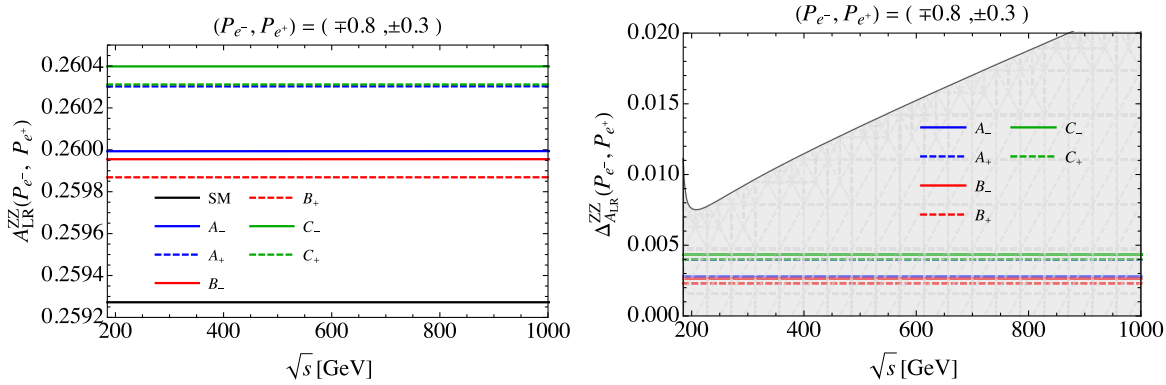

FIG. 13. The $\sqrt{s}$ dependence of the left-right asymmetry of the $e^-e^+ \to ZZ$ process and the deviation from the SM are shown. The left figure shows the $\sqrt{s}$ dependence of $A_{LR}^{ZZ}(P_{e^-}, P_{e^+})$ in the SM and the GHU model. The right figure shows the $\sqrt{s}$ dependence of $\Delta_{A_{LR}}^{ZZ}(P_{e^-}, P_{e^+})$, where $\Delta_{A_{LR}}^{ZZ}(P_{e^-}, P_{e^+}) \coloneqq [A_{LR}^{ZZ}(P_{e^-}, P_{e^+})]_{\mathrm{GHU}}/[A_{LR}^{ZZ}(P_{e^-}, P_{e^+})]_{\mathrm{SM}} - 1$. The energy ranges $\sqrt{s}$ in the first and second figures are $\sqrt{s} = [200, 3000]$ GeV, $\sqrt{s} = [200, 1000]$ GeV, respectively. The gray region represents the 1σ statistical error in the SM at each $\sqrt{s}$ with 1 ab^{-1} for each polarized initial states $(P_{e^-}, P_{e^+}) = (\mp 0.8, \pm 0.3)$ by using the total cross section of W boson pair production.

differential cross section including all the contribution from t-channel, u-channel, and interference terms. t-channel, u-channel, and interference stand for cross section only including each contribution. The right figure shows the $\sqrt{s}$ dependence of $\sigma^{WW}(P_{e^-}, P_{e^+})$ in the SM and the GHU model whose parameters set are $A_\pm$, $B_\pm$, $C_\pm$. From the left figure, we can see that for larger $\sqrt{s}$, stronger cancellation between t-channel, u-channel, and interference terms is taking place. This figure shows the SM case, but the same phenomenon occurs in the GHU model. From the right figure, we find that the cross sections in the GHU with the parameter sets $A_\pm$, $B_\pm$, $C_\pm$ are almost the same as that in the SM.

In Fig. 12, the $\sqrt{s}$ dependence of the deviation from the SM in the GHU models for the total cross sections, $\Delta_\sigma^{ZZ}(P_{e^-}, P_{e^+})$, is shown, where $\Delta_\sigma^{WW}(P_{e^-}, P_{e^+})$ is given in Eq. (4.72). The statistical errors in the SM are estimated by by using leptonic decays $Z \to \ell^+\ell^-$. Since $\mathrm{Br}(Z \to \ell^+\ell^-) = (3.3658 \pm 0.0023)\%$ [12], the branching ratio of $ZZ \to \ell^-\ell^+\ell'^-\ell'^+$ is 1.019%. The decay mode of Z bosons into charged leptons does not produce a sufficient number of events. If the decay of Z bosons into hadrons can be used with sufficient abundance and precision, it is possible that this process could be used to explore well beyond the limits from the LHC experiment into the m_{KK} region.

In Fig. 13, the $\sqrt{s}$ dependence of the left-right asymmetry A_{LR}^{ZZ} of the $e^-e^+ \to ZZ$ processes and the deviation from the SM $\Delta_{A_{LR}}^{ZZ}$ are shown, where A_{LR}^{ZZ} and $\Delta_{A_{LR}}^{ZZ}$ are given in Eqs. (4.73) and (4.75), respectively. The 1σ statistical error in the SM at each $\sqrt{s}$ with 1 ab^{-1} for each polarized initial electron and positron $(P_{e^-}, P_{e^+}) = (\mp 0.8, \pm 0.3)$ is estimated by using leptonic decays $Z \to \ell^+\ell^-$. As the same as the total cross section, the decay mode of Z bosons into charged leptons does not produce a sufficient number of events. If the decay of Z bosons into hadrons can be used with sufficient abundance and precision, it is possible that this process could be used to explore well beyond the limits from the LHC experiment into the m_{KK} region.

VI. SUMMARY AND DISCUSSIONS

In this paper we investigated the W and Z boson pair production processes in the $SU(3)_C \times SO(5)_W \times U(1)_X$ GHU model. First, by using the asymptotic behavior of the cross sections for large $\sqrt{s}$, we derived the conditions given in Eqs. (4.37) and (4.38) under which the $O(s)$ and $O(1)$ terms of the cross section for the $e^-e^+ \to W^-W^+$ process cancel. It is well known that these conditions are satisfied in the SM, but it is not obvious that the conditions are also satisfied in the GHU model because of the deviation of the coupling constants in the GHU model from those in the SM. We confirmed that even in the GHU model not only the condition in Eq. (4.37) related to the unitarity bound, but also the condition in Eq. (4.38) are satisfied with very good accuracy. Therefore, the unitarity bound is satisfied.

Next, we found that from Fig. 6 the deviation of the total cross section for the $e^-e^+ \to W^-W^+$ process from the SM in the GHU model with the parameter sets $A_\pm$, which are consistent with the current experimental constraints $(m_{\mathrm{KK}} \geq 13\ \mathrm{TeV}, \theta_H \leq 0.10)$, is about 0.5% to 1.5% and 0.6% to 2.2% for $\sqrt{s} = 250$ GeV and 500 GeV, respectively, depending on the initial electron and positron polarization. To estimate whether these deviation is actually observable or not, we estimated the statistical uncertainty by using the decay mode of $W^\pm$ decays into leptons. As a result, we found that it is possible to observe deviations from the SM in the GHU model with parameter sets whose KK mass scale is larger than 13 TeV.

From an analysis similar to the $e^-e^+ \to W^-W^+$ process, we also found that for the $e^-e^+ \to ZZ$ process the deviation from the SM in the GHU model is at most 1%. To estimate whether these deviation is actually observable or not, we estimated the statistical uncertainty by using the decay mode of Z bosons into charged leptons. Unfortunately, it is difficult to observe the deviation of cross sections from the SM in the GHU model by using the $e^-e^+ \to ZZ$ process because there is not a sufficient number of events.

In the GHU model, there is the large parity violation in the coupling constants of W' and Z' bosons to quarks and leptons. The bulk mass of the lepton determines whether the right-handed or left-handed coupling constant is larger. Therefore, the deviation of cross sections from the SM in the GHU model is expected to strongly depend on the initial polarization of electrons and positrons.

Further theoretical and experimental studies in the GHU model are necessary. As for theoretical studies, since the present study is a Born level analysis, there are various issues to be addressed to give more precise predictions, for example, off-shell final state contributions, initial-state radiation, QCD corrections, etc. Here we comment on the corrections to the $e^-e^+ \to W^-W^+$ process. The contributions of 1-loop corrections for the $e^-e^+ \to W^-W^+$ process in the SM and additional contributions from the $e^-e^+ \to W^-W^+\gamma$ whose γ is not detected are discussed in Ref. [101]. These effects lead to an $O(10)\%$ contribution to the $e^-e^+ \to W^-W^+$ process at tree level in the SM. Since the coupling constants in the GHU model are almost identical to those in the SM, this subleading contributions are expected to be almost the same as those in the SM. Therefore, the contributions to quantities defined from the ratio of cross sections, etc. in the SM and the GHU model such as $\Delta^{WW}_{d\sigma}$ and Δ^{WW}_{σ} in Figs. 4 and 6, in Figs. 4 and 6, for example, is expected to be small.

ACKNOWLEDGMENTS

This work was supported in part by the Ministry of Science and Technology of Taiwan under Grant No. MOST-111-2811-M-002-047-MY2 (N. Y.).

[1] T. Behnke, J. E. Brau, B. Foster, J. Fuster, M. Harrison, J. M. Paterson, M. Peskin, M. Stanitzki, N. Walker, and H. Yamamoto, The International Linear Collider technical design report—volume 1: Executive summary, arXiv:1306.6327.

[2] H. Baer, T. Barklow, K. Fujii, Y. Gao, A. Hoang, S. Kanemura, J. List, H. E. Logan, A. Nomerotski, M. Perelstein *et al.*, The International Linear Collider technical design report—volume 2: Physics, arXiv:1306.6352.

[3] C. Adolphsen, M. Barone, B. Barish, K. Buesser, P. Burrows, J. Carwardine, J. Clark, H. Mainaud Durand, G. Dugan, E. Elsen *et al.*, The International Linear Collider technical design report—volume 3.I: Accelerator R&D in the technical design phase, arXiv:1306.6353.

[4] C. Adolphsen, M. Barone, B. Barish, K. Buesser, P. Burrows, J. Carwardine, J. Clark, H. Mainaud Durand, G. Dugan, E. Elsen *et al.*, The International Linear Collider technical design report—volume 3.II: Accelerator baseline design, arXiv:1306.6328.

[5] H. Abramowicz *et al.*, The International Linear Collider technical design report—volume 4: Detectors, arXiv:1306.6329.

[6] A. Aryshev *et al.* (ILC International Development Team), The International Linear Collider: Report to Snowmass 2021, arXiv:2203.07622.

[7] L. Linssen, A. Miyamoto, M. Stanitzki, and H. Weerts, Physics and detectors at CLIC: CLIC conceptual design report, arXiv:1202.5940.

[8] A. Blondel and P. Janot, FCC-ee overview: New opportunities create new challenges, Eur. Phys. J. Plus **137**, 92 (2022).

[9] S. Dasu *et al.*, Strategy for understanding the Higgs physics: The cool copper collider, J. Instrum. **18**, P07053 (2023).

[10] M. Dong *et al.* (CEPC Study Group), CEPC conceptual design report: Volume 2—physics and detector, arXiv:1811.10545.

[11] C. Accettura *et al.*, Towards a muon collider, Eur. Phys. J. C **83**, 864 (2023).

[12] R. L. Workman *et al.* (Particle Data Group), Review of particle physics, Prog. Theor. Exp. Phys. **2022**, 083C01 (2022).

[13] Y. Hosotani, Dynamical mass generation by compact extra dimensions, Phys. Lett. **126B**, 309 (1983).

[14] Y. Hosotani, Dynamics of non-integrable phases and gauge symmetry breaking, Ann. Phys. (Amsterdam) **190**, 233 (1989).

[15] A. T. Davies and A. McLachlan, Gauge group breaking by Wilson loops, Phys. Lett. B **200**, 305 (1988).

[16] A. T. Davies and A. McLachlan, Congruency class effects in the Hosotani model, Nucl. Phys. **B317**, 237 (1989).

[17] H. Hatanaka, T. Inami, and C. S. Lim, The gauge hierarchy problem and higher dimensional gauge theories, Mod. Phys. Lett. A **13**, 2601 (1998).

[18] H. Hatanaka, Matter representations and gauge symmetry breaking via compactified space, Prog. Theor. Phys. **102**, 407 (1999).

[19] K. Agashe, R. Contino, and A. Pomarol, The minimal composite Higgs model, Nucl. Phys. **B719**, 165 (2005).

[20] A. D. Medina, N. R. Shah, and C. E. M. Wagner, Gauge-Higgs unification and radiative electroweak symmetry breaking in warped extra dimensions, Phys. Rev. D **76**, 095010 (2007).

[21] Y. Hosotani, K. Oda, T. Ohnuma, and Y. Sakamura, Dynamical electroweak symmetry breaking in $SO(5) \times U(1)$ gauge-Higgs unification with top and bottom quarks, Phys. Rev. D **78**, 096002 (2008).

[22] S. Funatsu, H. Hatanaka, Y. Hosotani, Y. Orikasa, and N. Yamatsu, GUT inspired $SO(5) \times U(1) \times SU(3)$ gauge-Higgs unification, Phys. Rev. D **99**, 095010 (2019).

[23] Y. Hosotani and N. Yamatsu, Gauge-Higgs grand unification, Prog. Theor. Exp. Phys. **2015**, 111B01 (2015).

[24] N. Yamatsu, Gauge coupling unification in gauge-Higgs grand unification, Prog. Theor. Exp. Phys. **2016**, 043B02 (2016).

[25] A. Furui, Y. Hosotani, and N. Yamatsu, Toward realistic gauge-Higgs grand unification, Prog. Theor. Exp. Phys. **2016**, 093B01 (2016).

[26] Y. Hosotani and N. Yamatsu, Electroweak symmetry breaking and mass spectra in six-dimensional gauge-Higgs grand unification, Prog. Theor. Exp. Phys. **2018**, 023B05 (2018).

[27] Y. Hosotani and N. Yamatsu, Gauge-Higgs seesaw mechanism in 6-dimensional grand unification, Prog. Theor. Exp. Phys. **2017**, 091B01 (2017).

[28] C. Englert, D. J. Miller, and D. D. Smaranda, Phenomenology of GUT-inspired gauge-Higgs unification, Phys. Lett. B **802**, 135261 (2020).

[29] C. Englert, D. J. Miller, and D. D. Smaranda, The Weinberg angle and 5D RGE effects in a SO(11) GUT theory, Phys. Lett. B **807**, 135548 (2020).

[30] H. Georgi and S. L. Glashow, Unity of all elementary particle forces, Phys. Rev. Lett. **32**, 438 (1974).

[31] K. Inoue, A. Kakuto, and Y. Nakano, Unification of the lepton-quark world by the gauge group SU(6), Prog. Theor. Phys. **58**, 630 (1977).

[32] H. Fritzsch and P. Minkowski, Unified interactions of leptons and hadrons, Ann. Phys. (N.Y.) **93**, 193 (1975).

[33] F. Gursey, P. Ramond, and P. Sikivie, A universal gauge theory model based on E_6, Phys. Lett. **60B**, 177 (1976).

[34] R. Slansky, Group theory for unified model building, Phys. Rep. **79**, 1 (1981).

[35] N. Yamatsu, Finite-dimensional Lie algebras and their representations for unified model building, arXiv:1511.08771.

[36] Y. Kawamura, Gauge symmetry breaking from extra space S^1/Z_2, Prog. Theor. Phys. **103**, 613 (2000).

[37] Y. Kawamura, Split multiplets, coupling unification and extra dimension, Prog. Theor. Phys. **105**, 691 (2001).

[38] Y. Kawamura, Triplet-doublet splitting, proton stability and extra dimension, Prog. Theor. Phys. **105**, 999 (2001).

[39] L. J. Hall and Y. Nomura, Gauge unification in higher dimensions, Phys. Rev. D **64**, 055003 (2001).

[40] L. J. Hall, Y. Nomura, and D. Tucker-Smith, Gauge Higgs unification in higher dimensions, Nucl. Phys. **B639**, 307 (2002).

[41] G. Burdman and Y. Nomura, Unification of Higgs and gauge fields in five-dimensions, Nucl. Phys. **B656**, 3 (2003).

[42] C. S. Lim and N. Maru, Towards a realistic grand gauge-Higgs unification, Phys. Lett. B **653**, 320 (2007).

[43] K. Kojima, K. Takenaga, and T. Yamashita, Grand gauge-Higgs unification, Phys. Rev. D **84**, 051701 (2011).

[44] K. Kojima, K. Takenaga, and T. Yamashita, Gauge symmetry breaking patterns in an SU(5) grand gauge-Higgs unification model, Phys. Rev. D **95**, 015021 (2017).

[45] K. Kojima, K. Takenaga, and T. Yamashita, The standard model gauge symmetry from higher-rank unified groups in grand gauge-Higgs unification models, J. High Energy Phys. 06 (2017) 018.

[46] N. Yamatsu, Special grand unification, Prog. Theor. Exp. Phys. **2017**, 061B01 (2017).

[47] N. Yamatsu, String-inspired special grand unification, Prog. Theor. Exp. Phys. **2017**, 101B01 (2017).

[48] N. Yamatsu, Family unification in special grand unification, Prog. Theor. Exp. Phys. **2018**, 091B01 (2018).

[49] N. Maru and Y. Yatagai, Fermion mass hierarchy in grand gauge-Higgs unification, Prog. Theor. Exp. Phys. **2019**, 083B03 (2019).

[50] Y. Kawamura, E. Kodaira, K. Kojima, and T. Yamashita, On representation matrices of boundary conditions in $SU(n)$ gauge theories compactified on two-dimensional orbifolds, J. High Energy Phys. 04 (2023) 113.

[51] S. Funatsu, H. Hatanaka, Y. Hosotani, Y. Orikasa, and N. Yamatsu, CKM matrix and FCNC suppression in $SO(5) \times U(1) \times SU(3)$ gauge-Higgs unification, Phys. Rev. D **101**, 055016 (2020).

[52] S. Funatsu, H. Hatanaka, Y. Hosotani, Y. Orikasa, and N. Yamatsu, Effective potential and universality in GUT-inspired gauge-Higgs unification, Phys. Rev. D **102**, 015005 (2020).

[53] S. Funatsu, H. Hatanaka, Y. Hosotani, Y. Orikasa, and N. Yamatsu, Fermion pair production at e^-e^+ linear collider experiments in GUT inspired gauge-Higgs unification, Phys. Rev. D **102**, 015029 (2020).

[54] S. Funatsu, H. Hatanaka, Y. Hosotani, Y. Orikasa, and N. Yamatsu, Electroweak and left-right phase transitions in $SO(5) \times U(1) \times SU(3)$ gauge-Higgs unification, Phys. Rev. D **104**, 115018 (2021).

[55] S. Funatsu, H. Hatanaka, Y. Hosotani, Y. Orikasa, and N. Yamatsu, Signals of W' and Z' bosons at the LHC in the $SU(3) \times SO(5) \times U(1)$ gauge-Higgs unification, Phys. Rev. D **105**, 055015 (2022).

[56] S. Funatsu, H. Hatanaka, Y. Hosotani, Y. Orikasa, and N. Yamatsu, Bhabha scattering in the gauge-Higgs unification, Phys. Rev. D **106**, 015015 (2022).

[57] S. Funatsu, H. Hatanaka, Y. Orikasa, and N. Yamatsu, Single Higgs boson production at electron-positron colliders in gauge-Higgs unification, Phys. Rev. D **107**, 075030 (2023).

[58] Y. Hosotani, S. Funatsu, H. Hatanaka, Y. Orikasa, and N. Yamatsu, Coupling sum rules and oblique corrections in gauge-Higgs unification, Prog. Theor. Exp. Phys. **2023**, 063B01 (2023).

[59] G. Aad *et al.* (ATLAS Collaboration), Search for high-mass dilepton resonances using 139 fb^{-1} of pp collision data collected at $\sqrt{s} = 13$ TeV with the ATLAS detector, Phys. Lett. B **796**, 68 (2019).

[60] G. Aad *et al.* (ATLAS Collaboration), Search for new non-resonant phenomena in high-mass dilepton final states with the ATLAS detector, J. High Energy Phys. 11 (2020) 005; 04 (2021) 142(E).

[61] G. Aad *et al.* (ATLAS Collaboration), Search for a heavy charged boson in events with a charged lepton and missing transverse momentum from pp collisions at $\sqrt{s} = 13$ TeV with the ATLAS detector, Phys. Rev. D **100**, 052013 (2019).

[62] G. Aad *et al.* (ATLAS Collaboration), Search for new resonances in mass distributions of jet pairs using 139 fb^{-1} of pp collisions at $\sqrt{s} = 13$ TeV with the ATLAS detector, J. High Energy Phys. 03 (2020) 145.

[63] A. M. Sirunyan *et al.* (CMS Collaboration), Search for high mass dijet resonances with a new background prediction method in proton-proton collisions at $\sqrt{s} = 13$ TeV, J. High Energy Phys. 05 (2020) 033.

[64] A. M. Sirunyan *et al.* (CMS Collaboration), Search for resonant and nonresonant new phenomena in high-mass dilepton final states at $\sqrt{s} = 13$ TeV, J. High Energy Phys. 07 (2021) 208.

[65] S. Funatsu, H. Hatanaka, Y. Hosotani, and Y. Orikasa, Distinct signals of the gauge-Higgs unification in e^+e^- collider experiments, Phys. Lett. B **775**, 297 (2017).

[66] J. Yoon and M. E. Peskin, Fermion pair production in $SO(5) \times U(1)$ gauge-Higgs unification models, arXiv:1811.07877.

[67] J. Yoon and M. E. Peskin, Dissection of an $SO(5) \times U(1)$ gauge-Higgs unification model, Phys. Rev. D **100**, 015001 (2019).

[68] S. Funatsu, Forward-backward asymmetry in the gauge-Higgs unification at the international linear collider, Eur. Phys. J. C **79**, 854 (2019).

[69] S. Bilokin, R. Pöschl, and F. Richard, Measurement of b quark EW couplings at ILC, arXiv:1709.04289.

[70] F. Richard, Bhabha scattering at ILC250, arXiv:1804.02846.

[71] A. Irles, R. Pöschl, F. Richard, and H. Yamamoto, Complementarity between ILC250 and ILC-GigaZ, in *Proceedings of the Linear Collider Community Meeting Lausanne, Switzerland* (2019), arXiv:1905.00220.

[72] A. Irles, R. Pöschl, and F. Richard, Production and measurement of $e^+e^- \to c\bar{c}$ signatures at the 250 GeV ILC, in *Proceedings of the International Workshop on Future Linear Colliders (LCWS 2019), Japan* (2019), arXiv:2002.05805.

[73] K. Fujii *et al.*, Physics case for the 250 GeV stage of the International Linear Collider, arXiv:1710.07621.

[74] H. Aihara *et al.* (ILC Collaboration), The International Linear Collider. A global project, arXiv:1901.09829.

[75] P. Bambade *et al.*, The International Linear Collider: A global project, arXiv:1903.01629.

[76] R. Pöschl (ILC International Development Team Working Group 3), Top and heavy quark studies at linear colliders, Proc. Sci. EPS-HEP2021 (**2022**) 491.

[77] A. Irles, R. Pöschl, and F. Richard, Experimental methods and prospects on the measurement of electroweak b and c-quark observables at the ILC operating at 250 GeV, arXiv:2306.11413.

[78] A. Irles and J. P. Marquez, Experimental prospects for precision observables in $e^-e^+ \to q\bar{q}$ with $q = b,\ c$ processes at the ILC operating at 250 and 500 GeV of center of mass, in *Proceedings of the International Workshop on Future Linear Colliders* (2023), arXiv:2307.14888.

[79] B. Schrempp, F. Schrempp, N. Wermes, and D. Zeppenfeld, Bounds on new contact interactions from future e^+e^- colliders, Nucl. Phys. **B296**, 1 (1988).

[80] D. C. Kennedy, B. W. Lynn, C. J. C. Im, and R. G. Stuart, Electroweak cross-sections and asymmetries at the Z^0, Nucl. Phys. **B321**, 83 (1989).

[81] K. Abe *et al.* (SLD Collaboration), Precise measurement of the left-right cross-section asymmetry in Z boson production by e^+e^- collisions, Phys. Rev. Lett. **73**, 25 (1994).

[82] K. Abe *et al.* (SLD Collaboration), An improved measurement of the left-right Z^0 cross-section asymmetry, Phys. Rev. Lett. **78**, 2075 (1997).

[83] T. Aaltonen *et al.* (CDF Collaboration), High-precision measurement of the W boson mass with the CDF II detector, Science **376**, 170 (2022).

[84] M. Froissart, Asymptotic behavior and subtractions in the Mandelstam representation, Phys. Rev. **123**, 1053 (1961).

[85] P. Langacker, *The Standard Model and Beyond* (Taylor & Francis, London, 2017).

[86] J. M. Cornwall, D. N. Levin, and G. Tiktopoulos, Derivation of gauge invariance from high-energy unitarity bounds on the S matrix, Phys. Rev. D **10**, 1145 (1974); **11**, 972(E) (1975).

[87] M. S. Chanowitz and M. K. Gaillard, The TeV physics of strongly interacting W's and Z's, Nucl. Phys. **B261**, 379 (1985).
[88] M. E. Peskin and D. V. Schroeder, *An Introduction to Quantum Field Theory* (Addison-Wesley, Reading, USA, 1995), p. 842.
[89] S. Funatsu, H. Hatanaka, Y. Hosotani, and Y. Orikasa, Collider signals of W' and Z' bosons in the gauge-Higgs unification, Phys. Rev. D **95**, 035032 (2017).
[90] L. Randall and R. Sundrum, A large mass hierarchy from a small extra dimension, Phys. Rev. Lett. **83**, 3370 (1999).
[91] S. Funatsu, H. Hatanaka, Y. Hosotani, Y. Orikasa, and T. Shimotani, LHC signals of the $SO(5) \times U(1)$ gauge-Higgs unification, Phys. Rev. D **89**, 095019 (2014).
[92] S. Funatsu, H. Hatanaka, and Y. Hosotani, $H \to Z\gamma$ in the gauge-Higgs unification, Phys. Rev. D **92**, 115003 (2015).
[93] W. Alles, C. Boyer, and A. J. Buras, W boson production in e^+e^- collisions in the Weinberg-Salam model, Nucl. Phys. **B119**, 125 (1977).
[94] R. W. Brown and K. O. Mikaelian, W^+W^- and Z^0Z^0 pair production in e^+e^-, pp, $p\bar{p}$ colliding beams, Phys. Rev. D **19**, 922 (1979).
[95] R. W. Brown, D. Sahdev, and K. O. Mikaelian, $W^\pm Z^0$ and $W^\pm\gamma$ pair production in νe, pp, and $\bar{p}p$ collisions, Phys. Rev. D **20**, 1164 (1979).
[96] S. Frixione, P. Nason, and G. Ridolfi, Strong corrections to WZ production at hadron colliders, Nucl. Phys. **B383**, 3 (1992).
[97] R. Mertig, M. Bohm, and A. Denner, FeynCalc: Computer algebraic calculation of Feynman amplitudes, Comput. Phys. Commun. **64**, 345 (1991).
[98] V. Shtabovenko, R. Mertig, and F. Orellana, New developments in FeynCalc 9.0, Comput. Phys. Commun. **207**, 432 (2016).
[99] V. Shtabovenko, R. Mertig, and F. Orellana, FeynCalc 9.3: New features and improvements, Comput. Phys. Commun. **256**, 107478 (2020).
[100] G. Moortgat-Pick *et al.*, The role of polarized positrons and electrons in revealing fundamental interactions at the linear collider, Phys. Rep. **460**, 131 (2008).
[101] W. Beenakker *et al.*, WW cross-sections and distributions, in *Proceedings of the CERN Workshop on LEP2 Physics (followed by 2nd meeting, 15–16 June 1995 and 3rd meeting 2–3 November 1995)* (1996), arXiv:hep-ph/9602351.